Polymer strategies in perovskite solar cells

Anna Isakova[1] and Paul D. Topham[2]*

1. Chemical Engineering and Applied Chemistry, Aston University, Aston Triangle, Birmingham, B4 7ET, UK.
2. Aston Institute for Materials Research, Aston University, Birmingham, B4 7ET, UK

* Corresponding author: isakovaa@aston.ac.uk

Abstract

Since their emergence in 2013, perovskite solar cells have reached remarkable efficiencies exceeding 22%. Such rapid development of this technology has been possible, in part, due to the feed of ideas from previous research in organic photovoltaics (OPVs) and light emitting diodes (OLEDs). This comprehensive review discusses the various polymer strategies that have led to the success of perovskite devices: from hole and electron transporting materials to polymer templating agents. This review further covers how these strategies potentially serve to overcome the two major obstacles that stand in the way of global implementation of perovskite solar cells; stability and J-V curve hysteresis. Through reference and comparison of OPV, OLED and perovskite technologies, we highlight the need for a unified approach to establish appropriate control systems and ageing protocols that are necessary to further research in this exciting direction.

1. Introduction

Since the emergence of roll-to-roll printable organic photovoltaics (OPVs), OPV technology has attracted attention due to its multiple advantages over conventional inorganic-based solar panels: they are flexible, light-weight, inexpensive, produced in a facile and scalable manner, can be made transparent or semi-transparent, colour-tunable and can be readily integrated into steel or glass components during building construction. However, there are often doubts about the marketability of such devices due to two major concerns: low power conversion efficiency (PCE) and stability. Indeed, the best OPV devices at the time of writing boasted a PCE of 11.5%, whereas the maximum reported efficiency for crystalline silicon

panels is 25.6%.[1] The rapid development of perovskite organic-inorganic solar cells (PSCs)[2] since 2013 has already achieved a remarkable PCE of 22.1%,[1] comparable to that of crystalline Si cells, which has immediately placed large-scale printable PSCs as a potential candidate to replace conventional inorganic devices, or at least take their own specific niche in various applications from aerospace to consumer electronics.

The most commonly used perovskite absorber is a crystal of composition $CH_3NH_3PbX_3$, where X = Cl, Br or I (or $MAPbX_3$, where MA is methyl ammonium). The major properties of the perovskite crystal rendering it so effective for light harvesting are discussed in great detail elsewhere.[3–9] A typical device (Fig.1a-c) consists of a perovskite absorber sandwiched between two electrodes, where charge collection is facilitated by two intermediate layers, namely a hole transport layer and an electron transport layer. The HOMO/LUMO levels of $MAPbI_3$ of -4.0/-5.6 eV ensure a wide range of materials adopted from OLED and OPV research is suitable for both electron and hole extraction. Although PSCs evolved as another type of dye-sensitized solar cell (DSSC)[10], the materials that yielded the highest reported PCEs are those typically employed in OPVs.[11] Similarly to OPVs, devices can be either of conventional (the incident light arrives at the cathode side of the device) or inverted architecture (incident light arrives at the anode side). Mesoscopic devices employ a mesoporous TiO_2 (or ZrO_2, or Al_2O_3) layer as an electron-extraction scaffold[2,12] to increase the electron-collecting interfacial area. Generally, inverted devices have demonstrated higher PCE values, even without the incorporation of an HTL.[13–15]

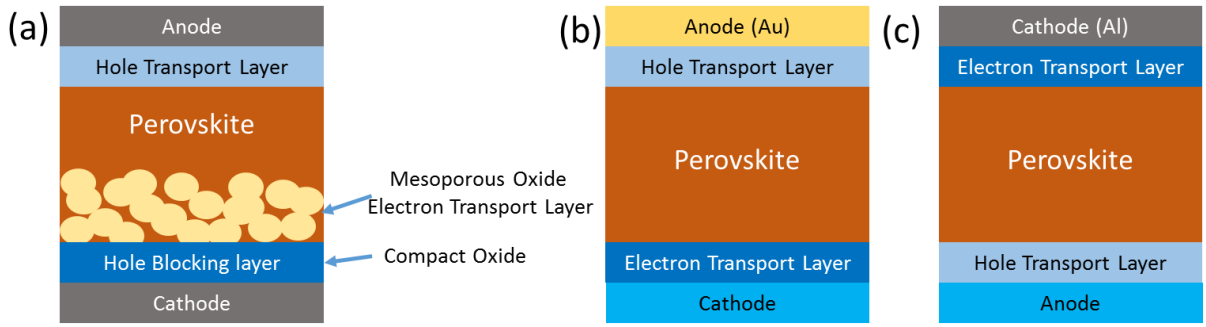

FIGURE 1. Typical schematic structures of perovskite devices: a) mesoscopic, b) planar conventional and c) planar inverted.

There are two major issues that prevent PSCs from global implementation: the current-voltage hysteresis of varying severity, with PCE values occasionally being dependent upon the scan direction and speed[16–18], and their inherent instability.[19] The first reported devices with high efficiency were rather unstable, with the perovskite absorber being especially susceptible to moisture in the air. In the presence of water, the perovskite decomposes to give lead halides, reducing photon absorption and its crystalline properties.

In OPV technology, polymers are widely employed throughout the entire device: from low band gap polymers and block copolymers in the active layer to interfacial materials and crosslinkers.[20–24] The modification of perovskite devices is performed mostly in the following directions: (i) improving the quality of the perovskite absorber films; (ii) enhancing charge transport across the interfaces; (iii) eliminating hysteresis and (iv) increasing the environmental stability of the devices. To note, the progression from a liquid electrolyte to a solid thin-film hole-transport material was the ground-breaking step that allowed all solid-state perovskites to achieve such high efficiencies.[25] In this review, we focus on reports of the use of polymers to boost the PCE and stability of PSCs. Efforts can be divided into three major groups: (i) polymeric hole transport materials (HTMs), (ii) polymeric electron transport materials (ETMs) and polymeric templating agents for assisted perovskite growth (Fig.2a). The first group of materials, polymeric HTMs, has received more attention and therefore a large component of this review is dedicated to that area.

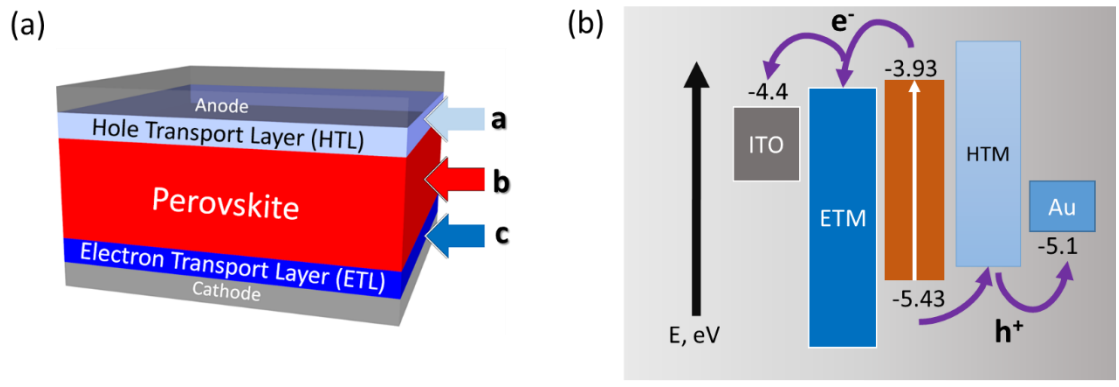

FIGURE 2. (a) Schematic representation for main layers targeted by polymeric strategies to improve the performance and stability of PSCs: (a) for hole transport, (c) for electron transport and (b) for

improvement of the perovskite absorber or m-TiO_2. (b) Lay-out of main energetic levels in a generalised perovskite device.

2. Hole transport materials

Hole transport in perovskite devices is one of the key processes that affects the overall PCE. Despite the perovskite film can transfer charges efficiently across its bulk, to avoid charge recombination at the interfaces, HTMs should also establish electron-blocking properties. Two major requirements for an efficient HTM is a HOMO level suitable to accept holes from the valence band of the perovskite (≥ -5.4 eV, Fig. 2b) and high hole mobility and conductivity.

One of the most prevalently used single molecule materials is spiro-OMeTAD (Fig.3), which has good solubility and combines fluorene and triarylamines moieties, enabling high hole mobilities in corresponding polymeric materials. Spiro-OMeTAD has a hole mobility ~ 1.69×10^{-6} $cm^2 V^{-1} s^{-1}$ in a thin film [26] and a HOMO level from -5.05 eV to -5.33 eV.[27] The conductivity of spiro-OMeTAD is high only in the oxidised state due to high level of oxygen doping,[28] with bis(trifluoromethane)sulfonimide lithium (Li-TFSI) salt[29] or cobalt (III) complexes.[30,31] 4-*tert*-Butylpyridine (tBP) has also been employed to increase hole mobility. The same dopants (structures presented in Fig.3) are also used to increase the conductivity of polymeric HTMs.

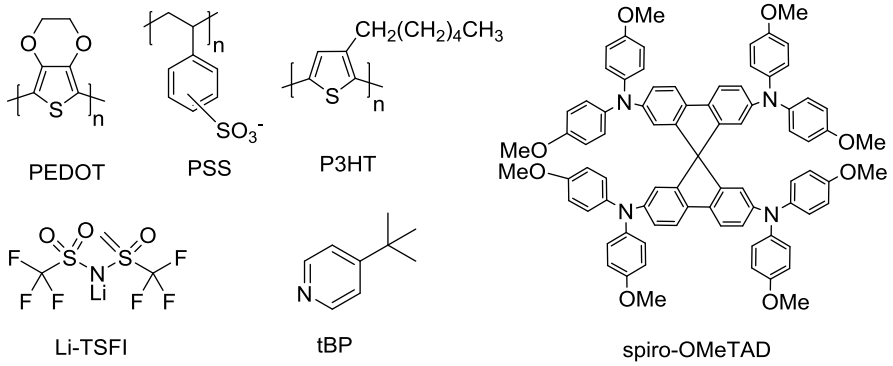

FIGURE 3. Chemical structures of polymers and small molecules, most often employed as HTMs.

Solid-state polymeric hole transport materials have been the subject of intensive research ever since the first reports of OLED and OPV technologies, thus by the time PSCs were introduced, there was a wide range of available polymeric materials: from conventional "synthetic metal", PEDOT:PSS, to low band

gap polymers and polytriarylamines. A summary of different materials, both doped and undoped, with corresponding PCE values and device architectures is presented in Table 1.

It is important to note that due to the variety of available device configurations and perovskite layer deposition techniques, comparing different HTMs directly remains a big challenge since the slightest alteration in perovskite deposition can often lead to an improved (or diminished) quality of film and therefore, drastically different efficiency values. Thus, authors often compare new HTMs to conventional PEDOT:PSS, P3HT or spiro-OMeTAD to demonstrate the superior performance of their latest devices. However, this does not imply that the same material will behave similarly in different device configurations or with perovskite deposited by a different approach. The major differences arise from the variation in quality of the perovskite film. In conventional planar devices, the HTM is deposited on top of the perovskite absorber. Then, high roughness of the perovskite (or very small grains) creates voids and gaps, allowing ingress of water and air into the active layer. Moreover, the contact between the HTM and perovskite will be poor and impede hole transfer. Additionally, such poor contact In inverted planar devices, the underlying HTM will define the quality of the perovskite layer deposited on top.[32,33] Mingzhu *et al* demonstrated that apparent hole mobility is different in a hole-only device to a complete perovskite device (from 1.91 x 10^{-4} cm^2 V^{-1} s^{-1} to 4.9 x 10^{-4} cm^2 V^{-1} s^{-1} for P3HT).[34] The difference was attributed to close intercalated contact between the HTM and the absorber, where the roughness of the layers, as well as their chemical interactions, plays an important role.

TABLE 1. Polymeric materials employed as HTMs in PSCs.

Polymer	HOMO/LUMO, eV	Charge mobility, cm^2 V^{-1} s^{-1}	Device (P-planar, M – mesoscopic)	Dopants/Additives	PCE	Ref
P3HT	-5.37/ -	1.3 x10^{-3}	P	Li-TFSI, tBP	12.4	35
P3HT	-	5.2x10^{-5}	P	gold nanoparticles	10.7	36
P3HT	-	-	P	-	10.4	37
PMC P3HT+	-	1.2x10^{-3}	M	Li-TFSI, tBP	17.7	34

Spiro-OMeTAD						
PEDOT:PSS	-	-	P	-	11.7	38
PEDOT:PSS		-	P	-	13.5	39
PEDOT:PSS		17.4	P	DMSO	10.2	40
PEDOT:PSS		-	P	PEO	16.8	33
PEDOT:PSS		-	P	TiO_2/MoO_3	13.6	41
PEDOT:PSS		-	P	GO	13.1	42
PEDOT:PSS	-5.4/ -	-	P	PFI	11.7	43
PEDOT	-5.11/ -	2.92	M	-	12.3	44
Low band gap polymers						
DPP (P)	-5.06/-3.68	1.95	P		10.0	45
PCDTBT	-5.5/-3.31		M		2.5	46
PCDTBT	-5.45/ -		M	Li-TFSI, tBP	4.2	47
PCPDTBT	-5.3/ -	$1x10^{-4}$	M	Li-TFSI, tBP	5.3	47
PDPP3T	-5.3/-3.74	$4x10^{-2}$	M	-	12.3	48
PDPPDBTE	-5.4/ -	$1x10^{-3}$	M	Li-TFSI, tBP	9.2	49
PTB7	-5.2/-3.31	$5.8x10^{-4}$	M	-	12.7	46
PTB7	-5.2/-3.31		M	Li-TFSI, tBP	13.3	46
PBDTTT-C	-5.12/-3.35	$2.4x10^{-4}$	P	-	9.9	50
PTB-DCB21	-5.22/-	$5.0x10^{-5}$	M	-	8.7	51
PDTSTTz-4	-5.0/-	$7.8x10^{-2}$	P	Li-TFSI, tBP	15.8	52
Polyfluorenes						
PFO	-5.8/-2.2	$1.5x10^{-4}$, $1.3x10^{-5}$	M	Li-TFSI, tBP	1.2	53
PFB	-5.1/-1.9	3×10^{-4}	M	Li-TFSI, tBP	8.0	53
TFB	-5.3/-1.9	$1x10^{-2}$, $7x10^{-3}$	M	Li-TFSI, tBP	10.9	53
Polytriarylamines and derivatives						

PTAA	-5.2/ -	4 x10-3	M	Li-TFSI, tBP	12.0	47
PTAA			M	Li-TFSI, tBP	16.2	54
PTAA			M $(FAPbI_3)_{1-x}$ $(MAPbBr_3)_x$	Li-TFSI, tBP	18.4	55
PTAA			M ($FAPBI_3$)	-	20.2	56
(poly)TPD	-5.4/-2.4		P	-	12.0	57
PTPD2	-5.26/ -	$4.7x10^{-4}$		Co(III) complex, Li-TFSI, tBP	5.1	58
HSL2 + PEDOT:PSS	-5.39/-2.41	$3.2x10^{-5}$	P	-	16.6	32
VNPB	-5.4		P	-	16.5	59
Other						
PANI nanoparticles	-5.27/ -		M	Li-TFSI, tBP	6.3	60
PANI-g-PSS:PFI	-5.39/-		P	-	12.4	61
$PVBT\text{-}SO_3$	-5.19/-	$2.67x10^{-3}$	P	-	15.9	

2.1 PEDOT:PSS

PEDOT:PSS has been adopted by the perovskite community from that of OPV devices, where it has been successfully used as the most appropriate hole transport material due to its high hole mobility ($17.4\ cm^2\ V^{-1}\ s^{-1}$) and conductivity.[62] PEDOT:PSS films are typically deposited from an aqueous suspension of various PEDOT to PSS ratios. This has been a major advantage of PEDOT:PSS when employed in OLEDs and OPVs since the deposition of subsequent layers from orthogonal solvents (water to o-dichlorobenzene/xylene) avoided washing away the underlying layers. For perovskites, however, this property can be a drawback, depending on the device configuration. The perovskite layer is moisture-sensitive, and although moisture treatment has been used to improve the film quality through controlled erosion of the layer,[63] any uncontrolled exposure can deteriorate the contact between layers and decrease the performance of the device. Moreover, PEDOT:PSS devices will always be more susceptible to

moisture-induced degradation due to the hygroscopic nature of the material.[19,64] In spite of the stability concerns, PEDOT:PSS remains one of the most attractive and best studied materials for hole extraction due to its availability in large batches, low cost and high transparency. Importantly, many modifications are available to tune its properties: from altering the content by chemical or mechanical treatment[65] to doping.[33]

First of all, the content of PSS in PEDOT:PSS suspensions can be varied to achieve a tunable work function.[38] For instance, suspensions with higher PSS content (1:20 PEDOT:PSS) yielded a somewhat reliable PCE of 11.7% with insignificant hysteresis (V_{OC} ~0.9 V, J_{SC}~19.26 mA cm^{-2}, FF ~ 63%), resulting from the increased work function of 5.23 eV (as compared to 5.02 eV in 1:2.5 films). Raman spectroscopy studies suggested that tuning of the work function originates from conformational changes in the PEDOT chains leading to an increase in its local conductivity. More recently, Sin *et al* reported the effect of varying the hole mobility of the PEDOT:PSS layer on device performance, showing that devices with 1:2.5 PEDOT:PSS suspensions had higher PCE due to a remarkably higher conductivity of 882 S cm^{-1}.[40] Slightly different results to those of Chang *et al*, are attributed to the fact that Sin *et al* used DMSO to improve the wetting of their PEDOT:PSS suspensions, which obviously had an effect on the chain packing and decreased the interchain mobility in the HTM. This observation highlights the sensitivity in perovskite device fabrication, since slightest variations in the fabrication procedures can yield drastically different results.

Another option for tuning the properties of PEDOT:PSS is to dope it with nanoparticles or conductive oxides. Li *et al* reported an efficient way to improve the conductivity of PEDOT:PSS by glycerol doping,[66] resulting in a 127-fold conductivity increase in films with 6% dopant content. The surface roughness increased with doping, resulting in better contact of the HTM with the perovskite absorber and therefore an enhancement of PCE from 8.6% in undoped PEDOT:PSS to 11.0% in 6% doped films was observed.

A significant increase in efficiency, up to 16.5%, was demonstrated when PEDOT:PSS was doped with PEO (Fig.4).[33] The main reason for this increase was associated with a remarkable improvement in

electrical conductivity from 0.2 cm^2 V^{-1} S^{-1} for pristine PEDOT:PSS to 348 cm^2 V^{-1} S^{-1} in 1.2% doped PEDOT:PSS. The external quantum efficiency of the PEO-doped devices in the range of 450 to 800 nm increased from 60% to more than 80% (Fig.4b), resulting in a J_{SC} value of 23.42 mA cm^{-2}. Importantly for large scale fabrication, devices with doped PEDOT:PSS demonstrated improved reproducibility and insignificant hysteresis of only 1.4% deviation between different scan directions (Fig.4c). Moreover, the low cost of PEO and the facile fabrication process of planar devices makes this material very attractive for large scale manufacturing.

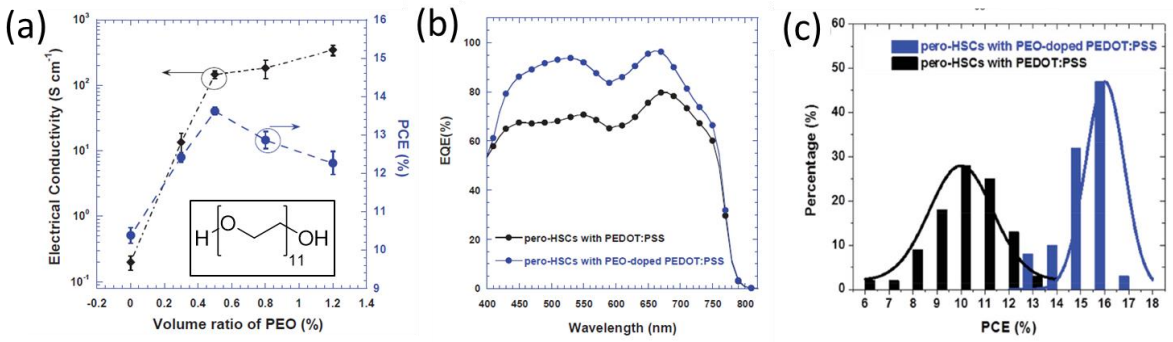

FIGURE 4. Effect of PEO doping on **(**a) electrical conductivities of PEDOT:PSS layer and device PCE values at varying PEO contents (chemical structure of PEO is presented in the inset), (b) the external quantum efficiency spectra and (c) reproducibility of the overall device performance (histograms of photovoltaic parameters for PEO-doped (blue) and undoped (black) devices). Adapted from [33] with permission from Wiley.

Li *et al* reported that an additional ultrathin layer of graphene oxide deposited between the ITO and PEDOT:PSS layers in a conventional architecture allowed a PCE of 13.1% to be attained (V_{OC} of 0.96 V, J_{SC} of 17.96 mA cm^{-2} and FF of 76%).[42] The graphene oxide layer has a very high electron blocking capacity and, thus, leads to supressed recombination at the interface. A similar approach of using an intermediate layer of molybdenum oxide (MoO_3) between the ITO and PEDOT:PSS improved the device efficiency from 9.81% to 12.78%.[67] This PCE further improved to 14.87% after 100 h storage under ambient conditions in the dark, associated with continuing growth of the perovskite layer during storage.

Another approach demonstrated by Liu *et al* exploited TiO_2/MoO_3 core/shell nanoparticles as a dopant for PEDOT:PSS in planar devices.[41] The doping resulted in a better, more compact morphology of the perovskite layer (Fig.5a-b) deposited on top of this HTM, since the nanoparticles served as nucleation sites for perovskite growth. The perovskite grains had less pinholes and reached 300 nm in diameter. The overall increase in PCE in 20% doped devices to 13.63% (J_{SC} of 17.35 mA cm^{-2}, V_{OC} of 0.96 V, FF of 84%) is, however, difficult to attribute only to perovskite morphology, since the mobility and conductivity of the resulting HTM were not studied. It is also unclear if the MoO_3 outer shell contributed to the charge carrier density through ground state doping, which was had been observed by other groups before. [59] The devices also demonstrated improved stability, retaining 92% of the maximum PCE after 400 h of storage in ambient air in the dark against only 19% retained in undoped devices (Fig.5c). The compact morphology of the perovskite absorber, as well as the reduced hygroscopic nature of the doped PEDOT:PSS layer, are deemed as the major reasons for the higher stability.

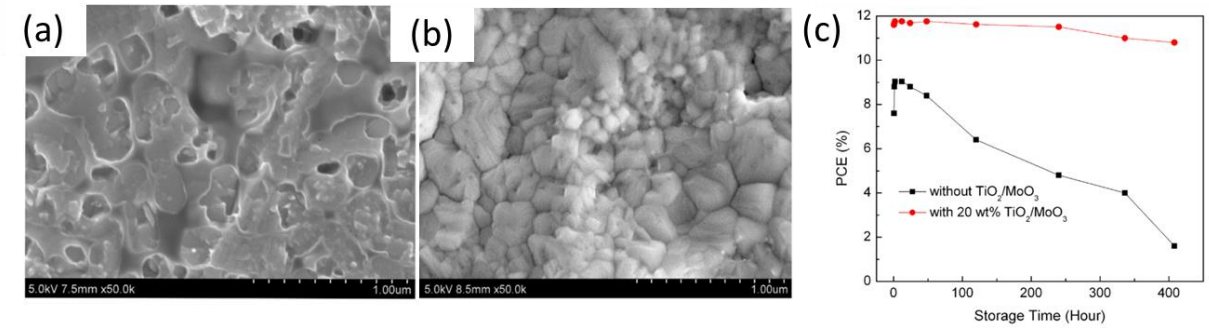

FIGURE 5. Application of TiO_2/MoO_3 core/shell nanoparticles for improvement of perovskite morphology. Top-view SEM images of $CH_3NH_3PbI_{3-x}Cl_x$ films deposited on (a) PEDOT:PSS and (b) 20% TiO_2/MoO_3-doped PEDOT:PSS layers. (c) PCE as a function of storage time under ambient conditions in the dark for devices with (red) and without (black) TiO2/MoO3 dopant in PEDOT:PSS layer. Adapted from [41], Copyright 2016 with permission from Elsevier.

PEDOT:PSS can be enriched with perfluorinated ionomers (PFI, Fig.6a) resulting in a self-organizing HTM (also referred to as self-organised hole extracting layer, SOHEL), which has been shown to improve the efficiency to 11.7% (J_{SC} of 16.7 mA cm^{-2}, V_{OC} of 0.982 V, FF of 70.5%) from 8.1%.[43] This improvement was associated with an increase in work function of the HTM from 4.86 eV in pristine

PEDOT:PSS to 5.4 eV in a PFI/PEDOT:PSS composite layer. Further PCE of 8.0%, remarkable for flexible devices, was demonstrated for PSCs deposited onto a PET/ITO substrate, with a V_{OC} of 1.04 V, J_{SC} of 15.5 mA cm^{-2} and a slightly decreased FF of 49.9% (Fig.6c).

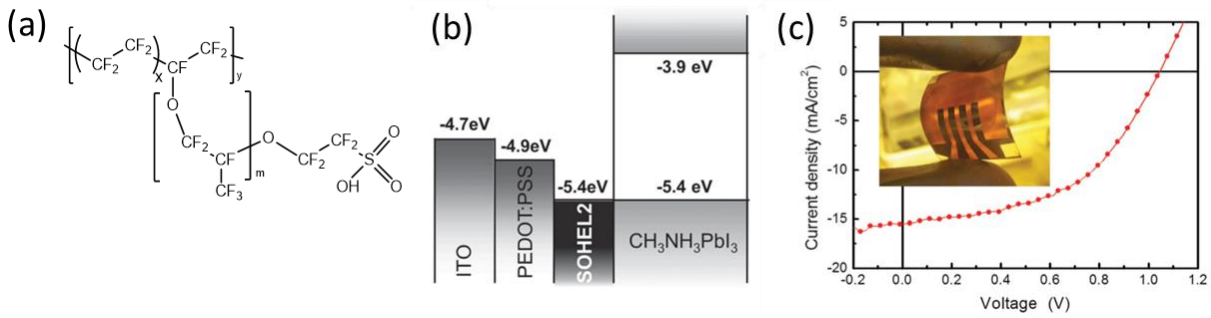

FIGURE 6. Application of a perfluorinated ionomer as an HTM. (a) Chemical structure of the PFI. (b) Schematic of the energy levels of each layer. (c) J-V curve of the flexible PSC with SOHEL2. The inset shows a device on a flexible PET/ITO substrate. Adapted from [43] with permission from Wiley.

An interesting concept of fabricating a bifacial device was reported by Xiao *et al*, who used electrogrown PEDOT as an HTM.[44] The film was deposited onto fluorine-doped tin oxide/glass substrate by cyclic voltammetry from aqueous solution, resulting in a PEDOT film approximately 250-300 nm thick. Further, a TiO_2-perovskite photoanode was clipped to the PEDOT/FTO electrode and the gap was filled with perovskite solution [44]. Interestingly, this very simple bifacial device yielded a PCE of 12.3% under the front end and 11.8% under rear end illumination. This is, to our knowledge, the first successful example of a bifacial approach in PSCs.

2.2 P3HT

Other polymeric materials adopted from OPV research are p-type organic semiconductors, such as P3HT and low-band gap donor polymers. Generally, P3HT, when used as an HTM, has demonstrated efficiencies superior to those of devices with low band-gap materials, with PCE values in the range of 10.4 to 17.7%.[34,35,37] The major reason for superior performance is the higher hole mobility and suitable HOMO levels (-5.37 eV), aligned with the valence band of the perovskite absorber.[68,69] Notably, previous studies have shown that the mobility of P3HT is highly dependent on its molecular mass.[68,69] Reported hole mobilities are in the range of 10^{-5} to 10^{-2} cm^2 V^{-1} s^{-1}, which can be further enhanced by doping with

tBP. The observed doping effect is associated with morphological changes in the P3HT layers, induced by the presence of tBP, which is a high boiling point solvent that enhances chain packing and crystallinity. Indeed, Guo and co-workers observed increased absorption at 561 and 610 nm in tBP-doped P3HT.[35] Li-TFSI dopant has a similar, yet less pronounced effect on the ordering of P3HT chains, although it is well-known to increase the charge carrier density rather than mobility through oxidative doping.

Two examples of particular note where P3HT has been used as HTM involve the use of so-called localized surface plasmon resonance effect, where the gold nanoparticles are employed to harvest red photons at their resonant frequency. Wang *et al* demonstrated that the addition of up to 20% gold nanoparticles resulted in a PCE enhancement by 25% (J_{SC} of 22.05 mA cm^{-2}, V_{OC} of 0.75 V, FF of 64.79 % and a resulting PCE of 10.71%).[36] The effect of doping P3HT was a complex one. Firstly, the nanoparticles improved chain ordering, as observed from an increased absorbance at 610 nm in doped P3HT films, and consequently led to a 2.5-fold increase in mobility. Secondly, the nanoparticles decrease the reflectance of incident light by scattering it within the device, thus extending the photon pathway and enhancing the absorption of the scattered photons by the perovskite (Fig.7). This scattering effect is confirmed by a 15% increase of incident photon-to-electron conversion efficiency in 20% doped P3HT devices. A similar approach has been proven to be efficient in doping PEDOT:PSS with gold nanoparticles, but for organic solar cells.[70–72]

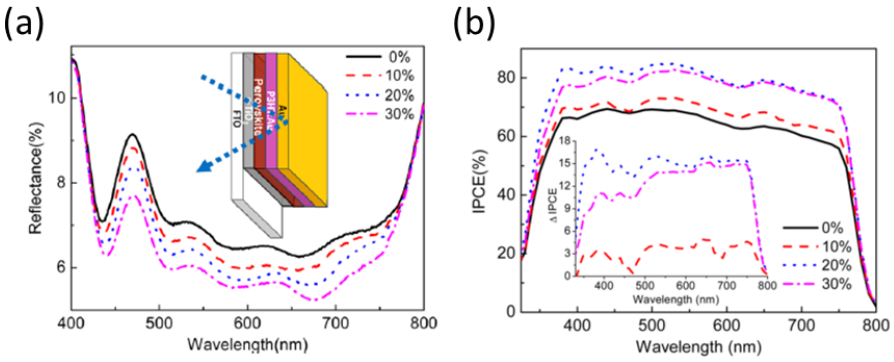

FIGURE 7. (a) Reflectance spectra of devices with and without incorporated gold nanoparticles with the inset showing a schematic illustration of the incident light path in a completed device. (b) Incident photon-

to-electron conversion efficiency curves for devices with different concentrations of gold nanoparticles in P3HT. Adapted with permission from [36]. Copyright 2015 American Chemical Society.

In parallel, Long *et al* reported PCE values of 17.7% (V_{OC} of 1.05 V, J_{SC} of 22.9 mA cm^{-2}, FF of 73.7%) in devices combining P3HT and spiro-OMeTAD to exploit the plasmon resonance effect in a different way. This combination resulted in a *quasi*-periodic microstructured HTM, which, in combination with the gold electrode, enabled the absorption of more red photons, allowing even thinner devices (240 nm) to be fabricated (Fig.8a-b).[34] The authors increased the cavity effect of the gold electrode by introducing a patterned HTM by simply mixing the two materials together and spin-coating the solution to give a self-assembled 3D cavity. In films deposited from a 3:1 spiro-OMeTAD:P3HT solution, spiro-OMeTAD aggregated into micro-embossements of 400-600 nm diameter (see AFM images in Fig.8c). The authors suggest that the solubility difference is one of the reasons for self-assembly, where the higher solubility of spiro-OMeTAD in o-dichlorobenzene leads to sequential precipitation of the components, however, the exact mechanism remains to be resolved (π-π interactions may contribute to the self-assembly process). The resulting plasmonic cavity effect indeed enhanced the absorption and thus increased the external quantum efficiency in the red region. Interestingly, the simulated plasmonic resonance peak originating from the self-assembled layer occurs at the same wavelength as the gold nanoparticles resonance peak from the study by Wang *et al* (at 530 nm). Furthermore, the self-assembled layer had an increased mobility of 1.2×10^{-3} cm^2 V^{-1} s^{-1}, almost one order of magnitude higher than individual mobilities of spiro-OMeTAD and P3HT, separately. Unfortunately, the reported devices showed pronounced hysteresis of up to 8% in 240 nm-thick devices, although still remarkably less hysteresis than in spiro-OMeTAD devices (up to 48%).

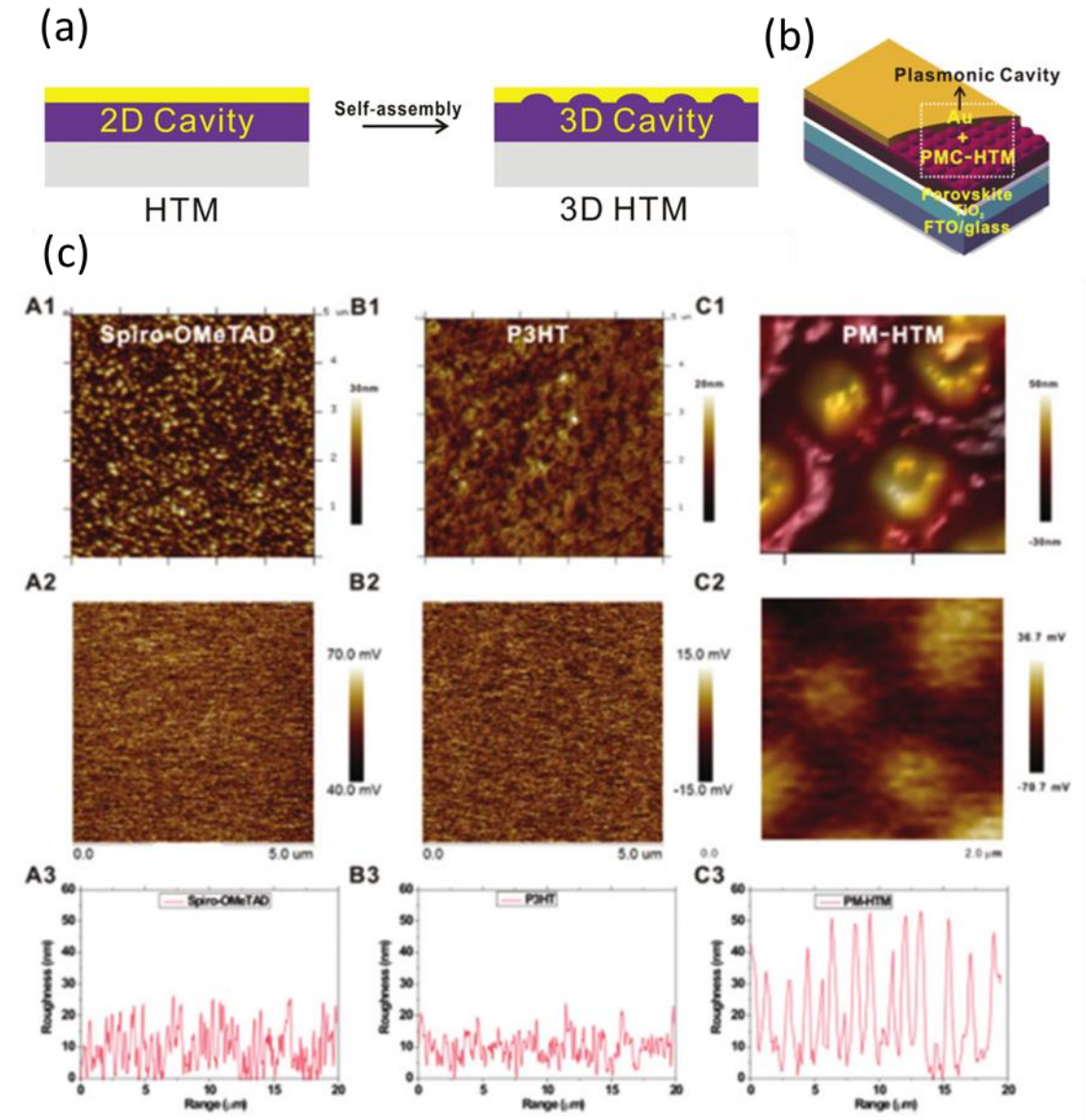

FIGURE 8. Strategy to enhance the red light deficiency using LSPR effect from self-assembled layer of P3HT and spiro-OMeTAD. (a) Schematic illustration of self-assembly process and (b) the resulting plasmonic cavity, formed by the self-assembled HTM and gold electrode. (c) Formation of the micro-embossments: (A1– C1) AFM surface morphologies, (A2–C2) surface relative potential and (A3–C3) roughness of the HTM films of spiro-OMeTAD, P3HT and resulting plasmonic HTM. Adapted from [34] with permission from The Royal Society of Chemistry.

2.3 Low band gap polymers

A wide range of low band gap polymers has been designed and tested for application in OPVs, with the major aim to improve the absorption of near-infrared photons. The structures of the low band gap

polymers employed in perovskite solar cells are presented in Fig.9. Low band gap polymers have reasonably high hole mobilities in the range of 10^{-5} to 10^{-3} cm^2 V^{-1} s^{-1}, where the mobility strongly depends on the organisation of the polymer in the film (*i.e.* its crystallinity/chain packing), and thus, on the processing parameters. Experiments on OPV optimisation have demonstrated that changes in solvent, additive or processing temperature and time have a huge impact on the crystallinity of low band gap polymers and development of structure in polymer films.[73]

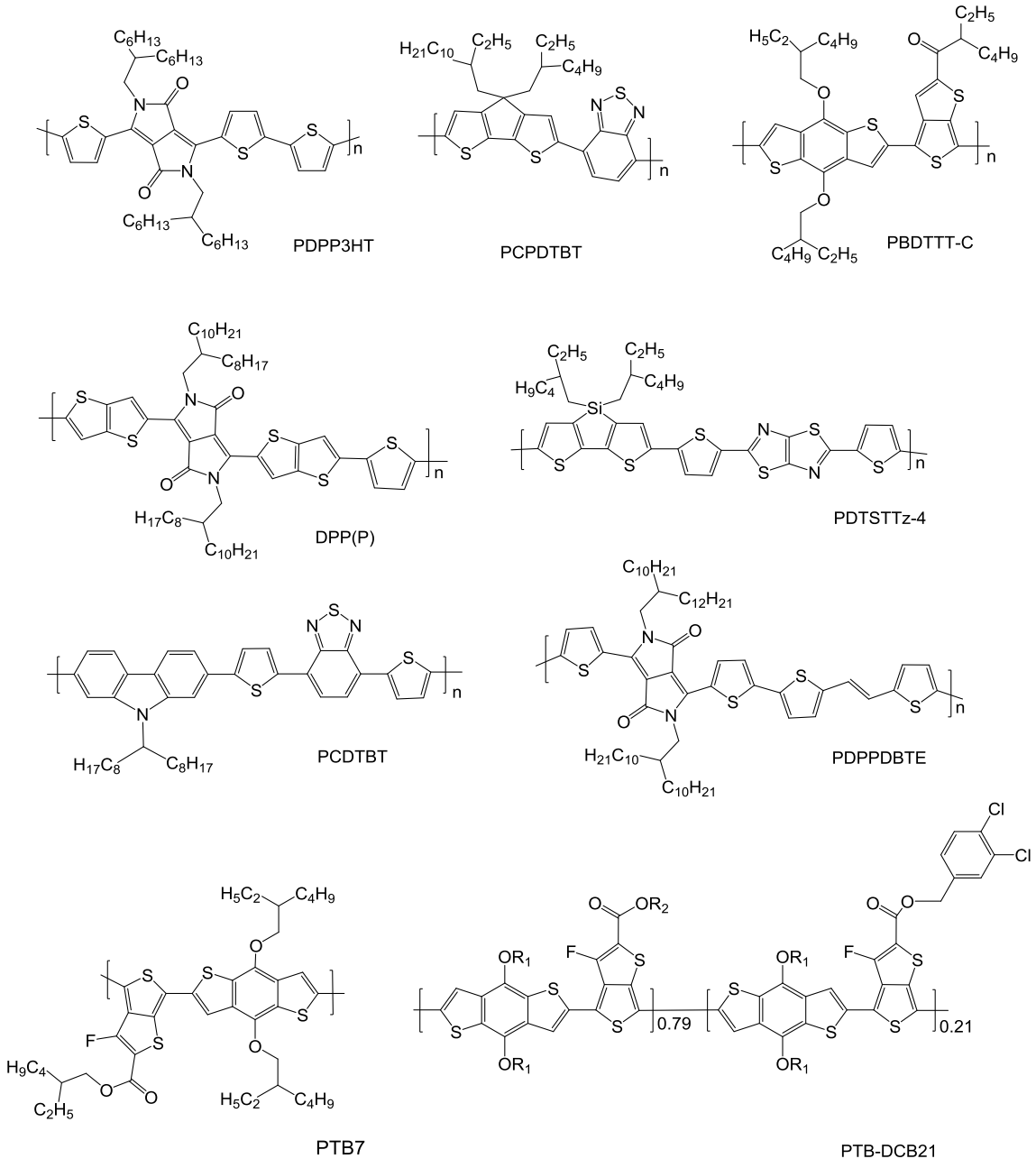

FIGURE 9. Chemical structures of low band gap polymers, used as HTMs in PSCs. For full polymer names the reader is directed to the glossary of this review.

Low band gap thiophene-based polymers, such as **PCPDTBT**, **PCDTBT** or **PCBTDPP** were systematically studied as HTMs in PSCs, but did not show any significant improvements in the PCE of mesoscopic perovskite devices, as shown by Heo and others.[47,74] Maximum PCE values reported for these polymers were in range of 4.2 -5.5%. The authors associated low PCEs with reduced chemical interactions between the polymers and perovskite, as well as with lower HOMO levels (-5.3 eV for PCPDTBT and -5.45 eV for PCDTBT).

On the other hand, a different thiophene-based donor polymer, **PTB7**, demonstrated a remarkably better device efficiency of 13.29% (J_{SC} of 20.2 mA cm^{-2}, V_{OC} of 0.94 and FF of 70%) after doping with Li-TFSI and tBP and device optimisation.[46] PTB7 had three-fold higher conductivity than P3HT (9.5 S/cm against 3.0 S/cm for P3HT) and almost five-fold higher than conventional spiro-OMeTAD (2.0 S/cm). Importantly, the authors showed that annealing of the perovskite layer in air led to an increase in grain size and consequently to better contact between the m-TiO_2 and absorber. PTB7 without dopants or air treatment resulted in a PCE of only 6.8% (with dopant 12.27%), whereas just air treatment boosted the PCE to 9.57%. These observations confirm the need to decouple the HTM-induced effects from those arising from improvements in the perovskite morphology.

Similar results were observed for another thiophene-based low-band gap polymer, **PBDTTT-C.**[50] PBDTTT-C was employed as an HTM in combination with conductive MoO_3 in a planar device, which allowed a maximum PCE of 9.95% to be achieved (J_{SC} of 17.68 mA cm^{-2}, V_{OC} of 0.87 V and FF of 64.83%). Lee *et al* reported the synthesis of a more elaborate thiophene-derived polymer denoted **PTB-DCB21** (Fig.10), with its mobility reaching 5.01 x 10^{-5} cm^2 V^{-1} s^{-1}. The dichlorobenzene-functionalised polymer demonstrated a higher PCE in mesoscopic devices than its non-functionalised analogue (8.7% against 7.4%).[51] The functionalised version exhibited faster electron transfer and lower recombination rates, which was attributed to better contact between the perovskite layer and HTM, originating from the π-cation and dipole-cation interactions between dichlorobenzene and perovskite absorber.

A number of research groups have explored the hole-transporting properties of diketopyrrolopyrrole-based polymers and their effect on the efficiency and stability of devices. Zhu *et al* achieved efficiency of 10.8% (J_{SC} of 18.47 mA cm^{-2}, V_{OC} of 0.88 V and FF of 67%) in simple ETM-free planar devices where **DPP(P)** was used as a thin HTM capping layer.[45] Another DPP-based polymer, **PDPPDBTE**, delivered a device efficiency of 9.2% (J_{SC} of 14.4 mA cm^{-2}, V_{OC} of 0.855 V and FF of 74.9%), which was higher than that of spiro-OMeTAD (7.6%) and P3HT-containing devices (6.3%).[49] Moreover, PDPPDBTE-based cells demonstrated a significantly improved stability without encapsulation, having lost only approximately 9% of the initial PCE value after 1,000 h of ageing (Fig.10a). This stabilisation was associated with the water repelling character of PDPPDBTE with a contact angle of 105°, much higher than that of spiro-OMeTAD. Importantly, P3HT, having the same contact angle as PDPPDBTE, demonstrated similar levels of stability in ambient conditions suggesting that HTMs with higher hydrophobicity could be beneficial for maintaining high performance of the devices for longer. Later, Dubey *et al* reported better mesoscopic devices with 12.32% PCE (J_{SC} of 20.5 mA cm^{-2}, V_{OC} of 0.98 and FF of 61.2%), incorporating undoped **PDPP3T** as HTM, however, devices also had marginally higher stability in air (Fig. 10b).[48]

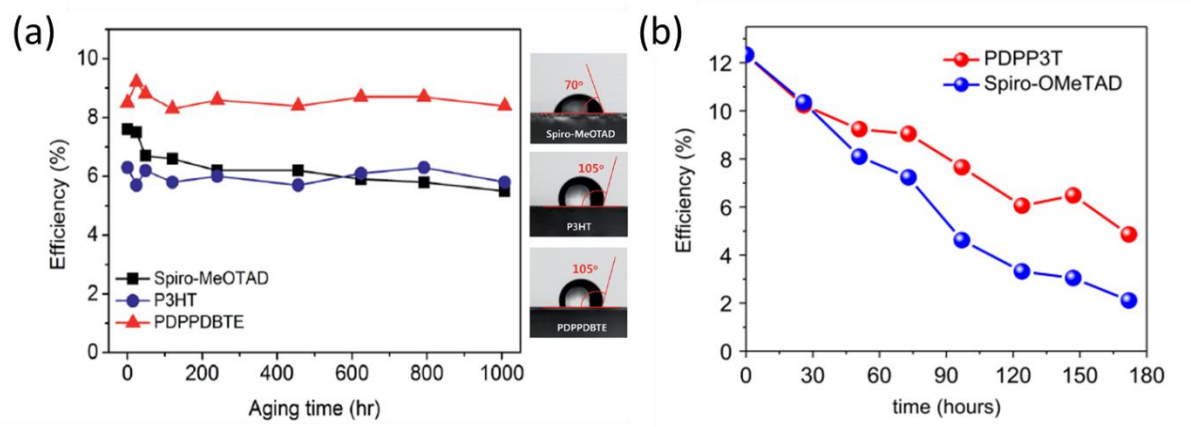

FIGURE 10. (a) Long-term stability of spiro-MeOTAD (black), P3HT (red), and PDPPDBTE (blue)-containing PSCs stored in 25% RH atmosphere. Corresponding water contact angles on an FTO substrate are given on the right. Adapted with modifications from [49] with permission from The Royal Society of Chemistry. (b) PCE as a function of storage time in ambient air for PDPP3T and spiro-OMeTAD-based devices. Reprinted from [48], Copyright 2016 with permission from Elsevier.

Alternatively, copolymers based on dithienosilole and thiazolothiazole (**PDTSTTz-4**) were studied as HTMs in inverted planar devices in order to increase absorption in the ultraviolet region.[52] These polymers have enhanced backbone planarity and, thus, improved chain stacking and increased mobility (up to 7.8 x 10^{-2} cm^2 V^{-1} s^{-1}). To compensate for charge carrier diffusion and facilitate electron extraction, Wang *et al* also introduced a thin layer of C60 fullerene between the c-TiO_2 and the active layer.[52] This combined strategy of employing two intermediate layers allowed to reach a PCE of 15.8% (J_{SC} of 22.39 mA cm^{-2}, V_{OC} of 0.97 V, FF of 72.6%) due to enhanced light harvesting in the 300-600 nm range and decreased interface resistance.

2.4 Polyfluorenes

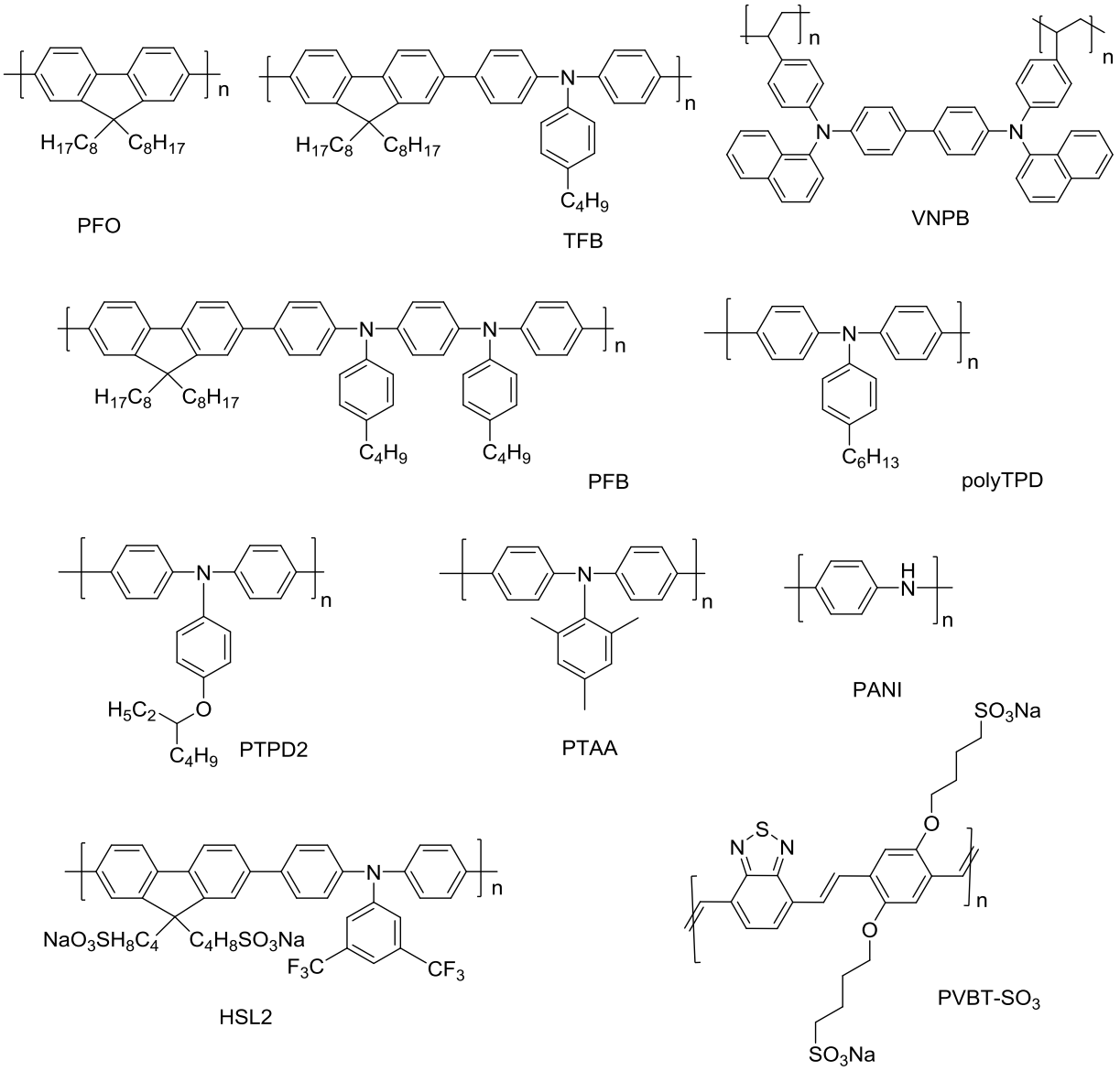

FIGURE 11. Chemical structures of other polymers used as HTMs in PSCs.

Polyfluorenes (see structures in Fig.11) and their derivatives are also capable of fast and efficient hole transport, as observed in OLED research.[75] The simplest polyfluorene, **PFO,** has a very low oxidation potential of -5.8 eV, which is below the valence band of the perovskite rendering hole extraction inefficient (PCE of devices only 1.22%).[53] However, changing the structure of PFO to incorporate an electron-rich triarylamine comonomer increases the HOMO level of the polymer (**TFB**) to -5.3 eV. With a more suitable HOMO level for the valence band of perovskite (-5.4 eV), TFB provided better interlayer hole transfer. Moreover, TFB demonstrated (i) a remarkably higher hole mobility (1×10^{-2} cm^2 V^{-1} s^{-1}) than that of PFO or spiro-OMeTAD and (ii) an exciton quenching efficiency very similar to that in spiro-OMeTAD devices (0.91 against 0.94). The combination of these factors resulted in a PCE of 10.92% (J_{SC} of 16.7 mA cm^{-2}, V_{OC} of 0.96 V and FF of 65%) in a mesoscopic device. obtained by a single-step perovskite deposition. However, in two-step deposition devices, TFB was not superior to spiro-OMeTAD (11.72% against 12.16% average PCE). Notably, **PFB**, an analogue of TFB with an even higher HOMO level of -5.1 eV, showed a slightly inferior efficiency (8.03% in one-step deposited devices) which was attributed to a reduction in photovoltage resulting from an excessively high HOMO level. These observations again stress how important is to decouple perovskite bulk effects from interfacial effects and their contributions to the overall device performance.

2.5 Polytriarylamines

The use of polytriarylamines [or poly(tetraphenylbenzidine)s] (**PTAAs**) in PSCs have been prompted by the OLED research where they are often employed as HTMs due to their low ionization potential and exceptional electron blocking properties, but typically low hole mobilities owing to the lack of long-range order and generally high amorphous content of the material.[76–78] Interestingly, despite PTAA being largely amorphous, its mobility in various cases depends on its molecular mass and dispersity, as often observed for semicrystalline materials.[69,79,80]. The mobility of PTAAs can also be increased by incorporating planar moieties, encouraging order in the films.[81]

Neumann *et al* studied the hole transporting properties of several PTAAs with different side chains.[58] Firstly, doping of the PTAAs with a cobalt (III) complex led to an order of magnitude increase in hole

mobility. Oxidation of the polymer was concluded to be the doping mechanism, which resulted in a higher density of cationic charge carriers, as shown by UV-Vis measurements. Indeed, PTPD2 doped with cobalt salt, when employed as an HTM, led to an increase in V_{OC}. Further doping with Li-TFSI and tBP improved the efficiency from 3.59% in undoped devices to 5.10 % (J_{SC} of 10.64 mA cm^{-2}, V_{OC} of 0.805 V and FF of 60%) in doped devices. Secondly, PTAAs with a hydrophilic side chain resulted in less pronounced J-V hysteresis than PTAAs with a hydrophobic alkyl chain. Devices were also much more photostable in air, with PCEs slightly increasing from 6.50 to 6.59% after five minutes of illumination (which could actually be the evidence of hysteretic behaviour), whereas the PTAAs with hydrophobic side chains lost almost 50% of the initial PCE value in this time. This study highlights the importance of tuning the polymer side chains not only to adjust HOMO/LUMO levels and morphology of the layers but also to increase the compatibility with underlying layers to serve towards improved stability. This concept of careful adjustment of the polymer side chains has been widely known for OPVs, but not yet fully explored for PSCs.[57]

The best PCE values so far have been obtained from devices incorporating simple methyl-substituted PTAA: from first reported by Heo *et al* PCE of 12.0% to 20.2% two years later.[47,55,56]. For example, a PCE of 18.4% was achieved when stable $MAPbI_3$ with a more efficient low-band gap absorber, formamidinium lead iodide ($FAPbI_3$).[55,82] This modification led to a PCE of 18.4% (J_{SC} of 22.5 mA cm^{-2}, V_{OC} of 1.11 V and FF of 73.2%) due to a significant improvement in the quality of perovskite layer (Fig.12).[55] Unfortunately, this latter approach gave rise to pronounced hysteresis, resulting in variations in PCE between 19.0% and 17.8% in different scanning directions.

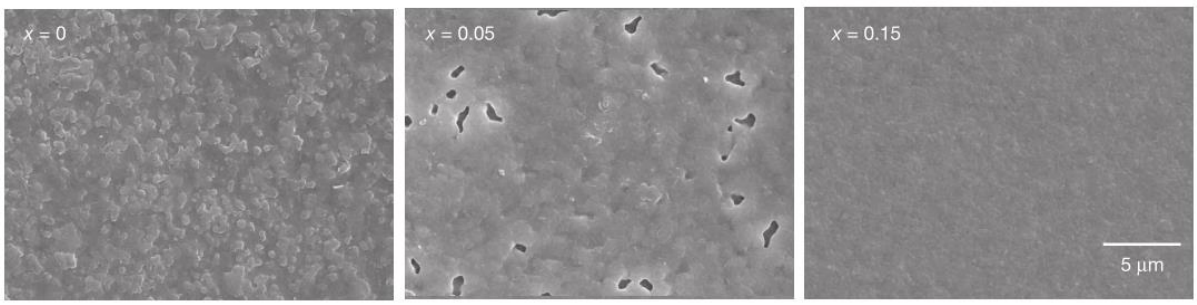

FIGURE 12. SEM images of $(FAPbI_3)_{1-x}(MAPbBr_3)_x$ films with different content of x = 50, 0.05 and 0.15. Reprinted by permission from Macmillan Publishers Ltd: [55], copyright 2015.

A remarkable example by Woon Seok Yang *et al* demonstrated that perovskite layer exploiting $FAPbI_3$ in an intermolecular exchange process with DMSO achieved a PCE of greater than 20% (20.2%, J_{SC} of 24.7 mA cm^{-2}, V_{OC} of 1.06 V and FF of 77.5%) with outstanding reproducibility.[56] Formation of the highly crystalline perovskite occurred through a distinct intermediate phase of FAI–PbI_2–DMSO, arising from non-covalent bonding between inorganic crystalline material and guest solvent molecules. The formamidinium ion has a similar size to that of a DMSO molecule, so DMSO molecules within a forming perovskite crystal can easily exchange for formamidinium ion without creating voids, pinholes or causing expansion. This strategy allowed smooth perovskite devices to be produced with large absorber grains and hysteresis-less photovoltaic characteristics.

Recently, a triarylamine polymer network of more elaborate structure was demonstrated as an HTM to enhance stability of PSCs. The triarylamine small molecule, **VNPB** (see structure in Fig.11), equipped with two vinyl moieties, was crosslinked to give a polymeric network, protecting the underlying perovskite layer from external stresses.[59] The crosslinked material also delivered another important advantage – it was solvent-resistant and would allow further deposition of layers in a hybrid device – a property that non-crosslinked materials do not possess. A thin layer of MoO_3 was deposited on top of VNPB to provide free hole density and therefore higher V_{OC} through efficient ground-state electron-transfer doping in the hole-transporting contact. Correspondingly, a charge transfer complex was observed in the UV-Vis spectrum in the near-infrared region at 800 nm and confirmed further by quenching of the photoluminescence in MoO_3/VBPB films (Fig. 13). The very same charge transfer can also be observed in spiro-MeOTAD films doped with lithium salts. However, as Xu *et al* have pointed out in their work, the major advantage of the VBPB/MoO_3 composite HTM is that only the functional interface is doped rather than the bulk film. The doping strategy resulted in a PCE of planar devices as high as 16.5%. Importantly, no hysteresis was observed in crosslinked devices. The device with crosslinked VBPB retained more than 95% of its initial efficiency after an hour of annealing at 100 °C. After 30 days in moist heat it did not show any stress-induced changes in the perovskite absorber. These findings show the potential of crosslinked HTMs to improve the efficiency and the stability of devices.[59]

Interestingly, UV-crosslinkable material with added photoinitiators delivered an inferior performance compared to that of spiro-OMeTAD devices. This was attributed to the erosion of the perovskite layer by the by-products of the degradation of the UV initiator.

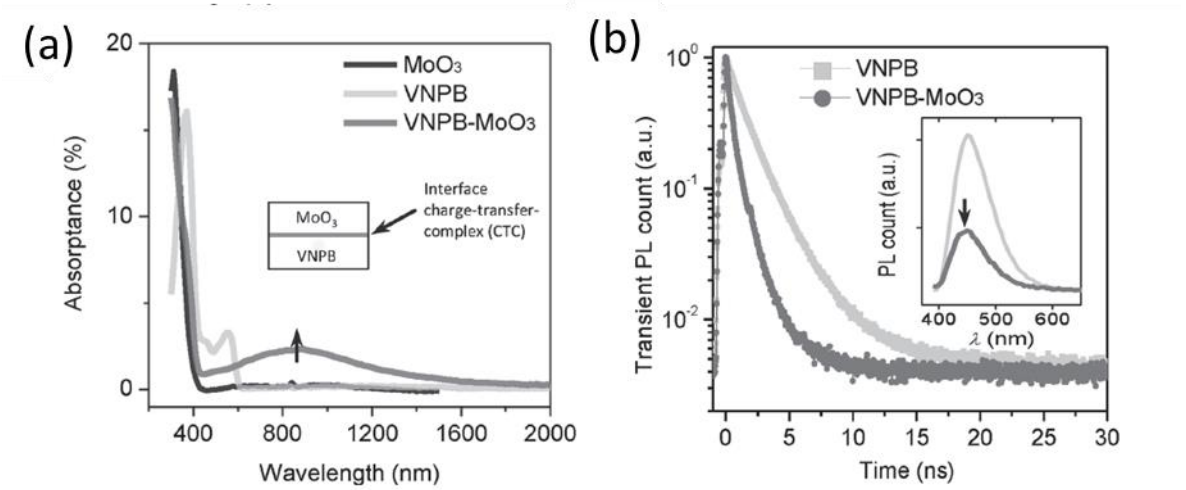

FIGURE 13. (a) Absorption spectra of MoO_3, VNPB and VNPB-MoO3 films, illustrating the charge transfer complex formed at the interface. (b) Photoluminescence spectra of VNPB and VNPB-MoO3 films. Photoluminescence quenching effect is induced by the interface charge-transfer-complex and observed in transient and steady-state measurements (inset) of VNPB. Reproduced from [59] with permission from Wiley.

A combination of hole transporting materials, including a layer of PEDOT:PSS and polytriarylamine-polyfluorene derivatives, was very recently reported by Xue *et al*, boosting the efficiency of conventional planar devices up to 15.4% and 16.6%, using non-fluorinated and fluorinated derivatives of the polytriarylamine-polyfluorene material, respectively denoted as HSL1 and HSL2.[32] New HTM layers had similar surface energies to the perovskite layer, which helped to improve the crystallinity and increase the grain size of the deposited absorber. Better contact between the HTM and active layer, with a reduced number of interfacial traps, led to insignificant (less than 1%) hysteresis being observed. However, as stand-alone HTMs, these polymers had poor hole mobilities of only 8.1×10^{-5} and 3.2×10^{-5} $cm^2\ V^{-1}\ s^{-1}$, for HSL1 and HSL2 respectively, which resulted in bad Ohmic contact between the layers and poor photovoltaic performance.

2.6 Polyanilines and other polymers

Polyanilines (**PANI**) have also been tested for their hole transporting properties due to their high conductivity.[83,84] For example, Ameen *et al* exploited PANI in the form of nanoparticles synthesised by oxidative chemical polymerisation, with an average size of 20 nm.[60] These nanoparticles penetrated into the perovskite thin film, resulting in a smoother surface and significant increase in the light absorbance of the device. The combination of these factors resulted in a maximum device PCE of 6.29% due to a J_{SC} of 17.97 mA cm^{-2}, V_{OC} of 0.877 V and FF of 40%. Such low fill factor originated from very high series resistance, as determined by impedance spectroscopy (~20.5 and ~41.2 Ω, with and without PANI, respectively). The authors also suggested that due to their shape, the PANI nanoparticles may increase the light scattering and thus, the absorbance of the incident light, however, no clear evidence for this was observed.

While improving the performance of their OLEDs, Choi *et al* developed a highly conductive PANI-based HTM, also containing PSS and PFI, where the PFI layer self-organised on top of a PANI:PSS layer upon deposition by spin-coating. This thin layer of PFI led to an increase in work function from 5.19 eV (in PANI:PSS only) to 5.98 eV in PANI:PSS:PFI (1:6:13.48 ratio).[85] This concept was further developed for application in perovskites where PANI was grafted onto PSS with a 1:6 PANI-to-PSS ratio.[61] The resulting **PSS-*g*-PANI** polymer had a work function of 4.99 eV, similar to that of PEDOT:PSS, but the V_{OC} of devices with PSS-*g*-PANI was higher than that in PEDOT:PSS devices (1.04 V and 0.923 V, respectively). Accordingly, the overall performance was better, with a PCE of 9.7% (against 7.8% in PEDOT:PSS devices). The increase in V_{OC} was associated with the higher HOMO level (5.39 eV) of PANI-*g*-PSS and a downshift in density of states below the Fermi-level. Doping of PSS-*g*-PANI with fluorinated PFI caused further downshift in surface energy below the Fermi level, and the V_{OC} increased to 1.07 V. Pristine PSS-*g*-PANI layers suffered from partial dissolution when the perovskite precursor PbI_2 was deposited on it, due to its high solubility in polar solvents, thus resulting in a decreased fill factor of 67.3%. However, when PSS-*g*-PANI was doped with PFI, which provided chemical resistance to polar solvents, the fill factor was higher than that of PEDOT:PSS devices (77.6% and 73%, respectively) and a PCE of 12.4% was attained.

A remarkable example of employing poly(arylene-vinylene)-based electrolytes, **PVBT-SO$_3$** (see structure in Fig.11), as an HTM was reported by Liu et al, where PVBT-SO$_3$ was deposited from an aqueous solution in a planar inverted device and used further without any annealing.[86] The polymer improved not only crystallinity of the perovskite layer, deposited on top of the HTM, but also the quality, resulting in a pinhole-free perovskite layer. Moreover, having a higher work function than PEDOT:PSS, PVBT-SO$_3$ resulted in higher built-in field across the devices. Thus, the average PCE of PVBT-SO$_3$ devices was 15.9% (V_{OC} of 0.97 V, J_{SC} of 21.2 mA cm^{-2} and FF of 77.4%), 26% higher than that of PEDOT:PSS devices.

Such a wide range of polymeric solutions is a result of extensive previous research in OPVs and OLEDs, which prompted the best ideas and helped the PSC technology to achieve high PCE values just in 3 years. It would not be unexpected if the feed started to work in the opposite direction, delivering successful ideas the OPV research, helping to boost currently poor performance of the organic flexible devices through incorporating new donor polymers or HTMs.

3. Electron transport materials

The configuration of devices dictates most appropriate approaches for efficient electron transport in PSCs. For instance, in mesoscopic devices, mp-TiO$_2$ acts as an electron transporter, whereas a compact non-porous TiO$_2$ layer provides hole-blocking properties. Efficiency of such devices can be improved by employing a thin interlayer, for example a self-assembled monolayer of a fullerene derivative which can efficiently passivate surface traps in TiO$_2$ and results in PCEs as high as 17.3%.[87] The structures of polymeric ETMs discussed further in this review are presented in Fig.14 and their properties are summarised in Table 2.

TABLE 2. Polymeric materials employed as ETMs.

Polymer	HOMO/LUMO, eV	HTM	Device type (C – conventional, I – inverted)	PCE, %	Ref
PN4N	-	PEDOT:PSS	C	15.0%	88

PFN-OX	-	Spiro-OMeTAD + LiTSFI+tBP	I	11.1%	89
PFN-OX+ZnO	-/-4.20	Spiro-OMeTAD + LiTSFI+tBP	I	15.5%	89
PFN-2TNDI	-5.58/-3.78	PEDOT:PSS	C	16.7%	90
N2200 (NDI2OD-T2)	-3.93/-5.66	PEDOT:PSS	C	8.78%	91
N2200 (NDI2OD-T2) + PCBM[a)]	-	PEDOT:PSS	C	10.57%	92
PNVT-8	-3.91/-5.60	PEDOT:PSS	C	7.74%	91
PNDI2OD-TT	-3.87/-5.73	PEDOT:PSS	C	6.47%	91
PPDIDTT[b)]	-3.90/-5.90	PEDOT:PSS	I	16.1%	93

(a) The polymer was employed as a blend with PCBM.

(b) The polymer was employed as an interfacial layer between perovskite and PCBM.

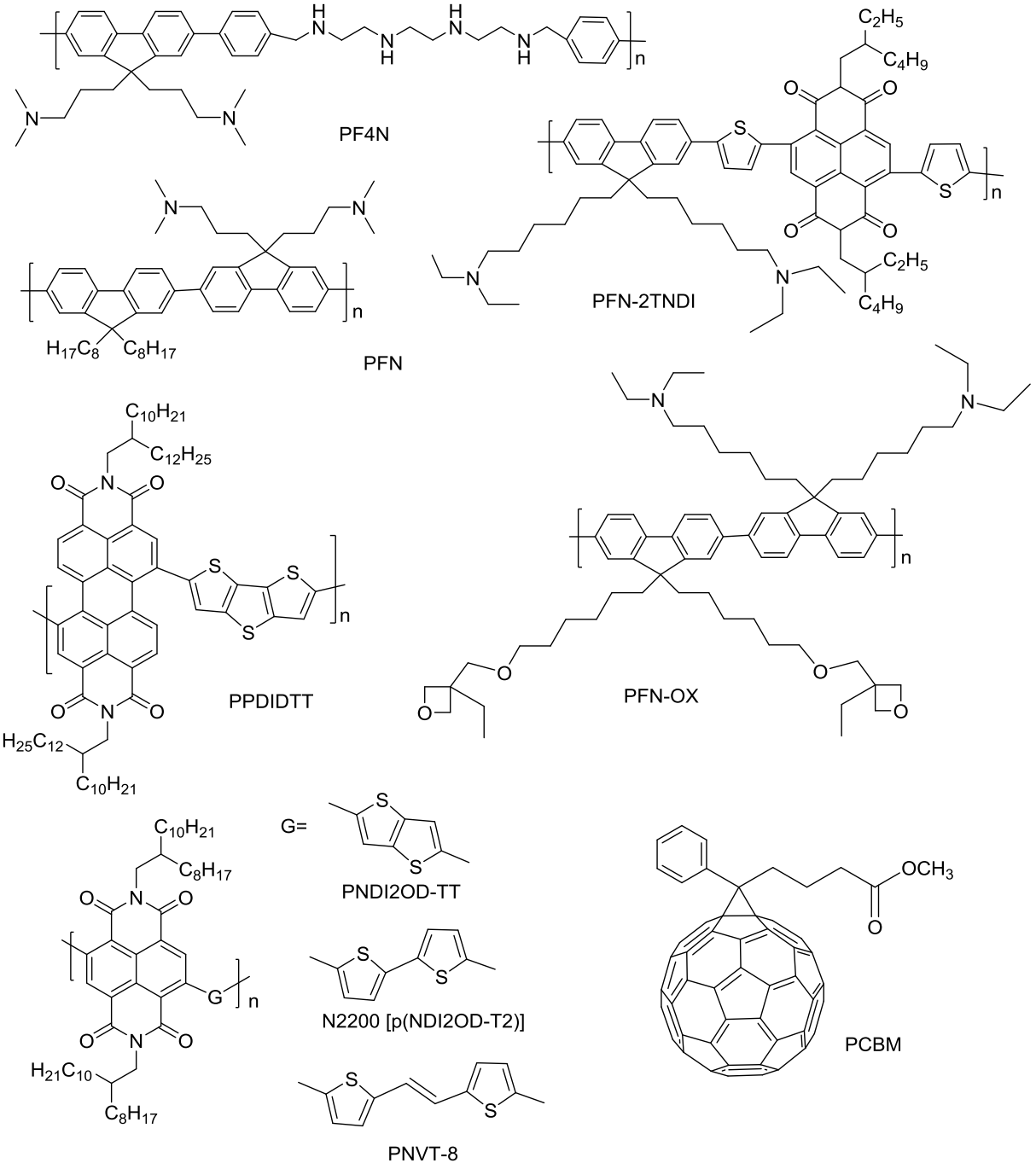

FIGURE 14. Chemical structures of polymers and small molecule PCBM employed as ETMs in PSCs.

In conventional planar devices, ETMs have many important functions beside transferring and transporting electrons. Firstly, the ETM serves as a substrate for deposition of the perovskite layer and thus, its surface energy defines the final quality of the films, among other factors. Secondly, its solvent resistance also plays an important role since any erosion of the underlying layer during deposition disrupts the

crystallinity of the formed perovskite and creates shunts and recombination sites at the interface. Thirdly, in inverted planar devices, the ETM is deposited onto the perovskite layer and should mediate good contact between the two layers by penetrating into the grain boundaries. Finally, the ETM is considered as one of the essential barriers against moisture and air penetration into the perovskite absorber, thus it should be highly hydrophobic to repel water.

One approach to improve both performance and stability of PSCs is to employ highly crosslinkable ETMs, such as those demonstrated by Qin Hu *et al*.[89] Their crosslinked layer played two major roles: (i) reducing the ingress of moisture into the device and (ii) increasing solvent resistance to avoid layer dissolution during the subsequent perovskite deposition from polar solvents, such as DMSO. To this end, a polyfluorene derivative furnished with an oxetane group (**PFN-OX**) was synthesised, where the oxetane group was capable of thermal crosslinking. Interestingly, although pristine **PFN** did not show solvent resistance to chlorobenzene as crosslinked PFN-OX did, PCE values obtained for planar conventional devices with PFN-OX were only marginally better – 10.2% for PFN and 11.1% for PFN-OX (J_{SC} of 18.7 mA cm^{-2}, V_{OC} of 0.94 V and FF of 63%). The PFN-OX/perovskite interface was further modified by depositing a thin (30 nm) layer of ZnO nanoparticles over the PFN-OX. This modification led to an increase in work function of the ETM to -4.2 eV, ideally suited to both the perovskite work function of -3.9 eV and that of ITO (-4.4.eV). Modified devices demonstrated PCEs of 15.5%, primarily owing to a significant increase in fill factor (from 63% in PFN-OX device to 75% in PFN-OX/ZnO device) and shunt resistant.

Xue *et al* also attempted to employ PFN in planar inverted devices.[88] However, it was not found suitable for interfacial modifications due to decomposition of the perovskite absorber by methanol, since PFN was deposited from this solvent. Consequently, PFN was synthetically modified to produce an IPA-soluble **PN4N**, which was used as a cathode interlayer between a PCBM ETM and aluminium electrode. Introduction of PN4N led to an enhancement of PCE from 12.4% to 15.0%, due to a significant increase in fill factor (from 62.5% to 72.5%).[88] The authors suggested that reduced leakage at the modified cathode interface was a major reason for the improvement in fill factor.

Another example employing an amino-functionalised polymer consisting of fluorene and naphthalene diimide units (**PFN-2TNDI**) achieved a PCE of 16.7% (with J_{SC} of 21.9 mA cm^{-2}, V_{OC} of 0.98V and FF of 78%) in conventional planar device, compared to that with PCBM as an ETM of 12.9%.[90] PFN-2TNDI has a LUMO level of -3.84 eV, closely matching the conductive band of the perovskite (-3.8 eV), and a deep HOMO level of -5.58 eV, sufficient for good hole-blocking performance. The authors stated that the amino group of the polymer had a strong passivation effect, reducing the trap states at the interface, since devices with polymers without amino groups (**PF-2TNDI**) did not demonstrate a pronounced photovoltaic effect (Fig.15).

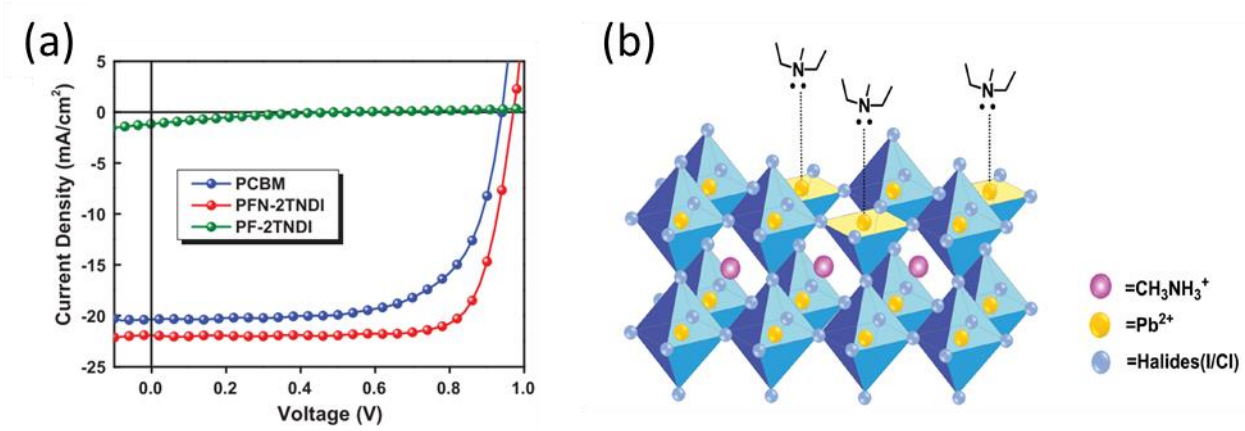

FIGURE 15. (a) J-V curves for the best-performing solar cells with PFN-2TNDI, PF-2TNDI (its analogue without amine groups) and PCBM as ETMs. (b) Schematic illustration of the potential surface defect sites of perovskite and the passivation effect of the amine groups. Adapted from [89] with permission from The Royal Society of Chemistry.

Electron-deficient naphthalene diimide (NDI) units have been incorporated into a polymer (**NDI2OD-T2**), which was employed at 10% ratio together with PCBM as an ETM.[92] The main idea was to achieve a homogeneous thin film by systematically varying the thickness of the films (by changing the spin speed) or contents of the layer. This combination of polymer and PCBM indeed resulted in a significant increase in external quantum efficiency, compared to those with only PCBM. Incorporation of a blended layer also helped to decrease trapped states (leading to mostly bimolecular recombination) as observed from a V_{OC}-light intensity plot. Conversely, in PCBM-containing devices recombination predominantly occurred

through trap states, worsening with decrease in thickness of the PCBM layer. The combination of these factors explained the enhancement of average PCE from 5.78% to 9.82% (with J_{SC} of 14.1 mA cm^{-2}, V_{OC} of 0.86 V and FF of 79.3%). Importantly, this study suggested that electron collection at the cathode can be further optimised by using polymers and polymer blends, rather than small molecules like PCBM that are susceptible to aggregation upon deposition and, thus, provide opportunities for creation of interfacial traps and pinholes. Other derivatives of the naphthalene diimides were tested as ETMs in conventional devices incorporating PEDOT:PSS as HTM, by Weiwei Wang *et al.*[91] They did not demonstrate any substantial improvements in performance (maximum PCE of 8.15% for N2200) compared to PCBM (maximum PCE of 8.51%).

Meng *et al* reported a perylene-based copolymer with dithienothiophene (**PPDIDTT**) as a dual functional interfacial layer, where the dithienothiophene unit passivates the surface trap states of the perovskite and the perylene unit serves for better charge transfer.[93] This polymer, introduced between electron-transporting PCBM and perovskite in a planar device, resulted in an average PCE of 16.1% (J_{SC} of 21.1 mA cm^{-2}, V_{OC} of 0.99 V and FF of 79.1%) against 14.7% in devices without the interfacial layer.

Clearly, in spite of various reports discussed above, the PCBM devices achieve the highest reported efficiencies (16-17%) of all ETMs.[87,94] Due to the shape and size of PCBM, it is capable of filling in the pinholes/gaps in the perovskite layer, facilitating electron collection and decreasing the number of traps, whereas the smooth polymer surfaces require the smooth perovskite, to establish optimal contact.[94]

4. Templating agents for perovskite growth

As demonstrated by multiple examples,[95] uniformity and homogeneity of the perovskite layer is the key to high device efficiency. However, obtaining a smooth, pinhole- and void-free perovskite film remains a non-trivial task. Procedures designed to facilitate uniform growth of the perovskite layer include sublimation,[57] solvent engineering,[54] and addition of surfactants[96] among others. Optimal conditions of perovskite processing result in a smooth surface with a large grain size and high perovskite crystallinity.

Polymers can play a significant role in providing optimal morphology of the absorber when they are used as a template to ensure the homogeneity of the precursor distribution in solution (or in suspension). For

example, Masi *et al* have tested various polymers as matrices for perovskite deposition, including PMMA, PS, PTAA, PFN and MEH-PPV.[97] The findings show that weak non-covalent interactions between polymer molecules and perovskite crystallites determine the aggregation character of crystals in the precursor solution and, thus, homogeneity of deposited films. For example, MEH-PPV interacted strongly with the MA^+ acid hydrogen atom through its ether groups, whereas PFN provided the nitrogen atoms with their lone pairs to establish hydrogen bonding. This bonding prevented the perovskite from excessive self-aggregation (Fig.16c). The significance of this study is that the nuclear magnetic resonance (NMR) time measurements provided unprecedented insight into the solution behaviour of the perovskite precursor and helped to predict the final film morphology. Films with homogenous morphology were formed upon deposition from solutions with a low spin-spin relaxation time (T2), e.g. T2 = 0.63 s for MEH-PPV:perovskite and 2.50 s for perovskite only. The same group further demonstrated application of the MEH-PPV:perovskite nanocomposites in complete devices, however, the reported PCE was only 3.0%.[98]

Addition of 1% of PEG or PEI had a positive effect on the morphology of the perovskite layer.[99,100] PEG helped to fill the voids which were formed during the phase transformation at elevated temperatures, and thus increased the coverage of TiO_2 by the perovskite absorber (Fig.16d). Closer contact between perovskite and ETM led to an increase in V_{OC} from 0.88 to 0.97 V. As a result, the efficiency of their best device also increased from 10.58% to 13.20%.[99] PEI acted similarly through improving the crystallinity of the perovskite films (Fig.16b). The presence of PEI supressed the carrier recombination, as seen by a remarkable increase in the photoluminescence intensity of the perovskite:PEI film, and a faster quenching of the generated excitons at the ETM:perovskite interface. Accordingly, addition of only 1% PEI resulted in a 26% improvement of PCE (from 11.17% to 14.07%).[100]

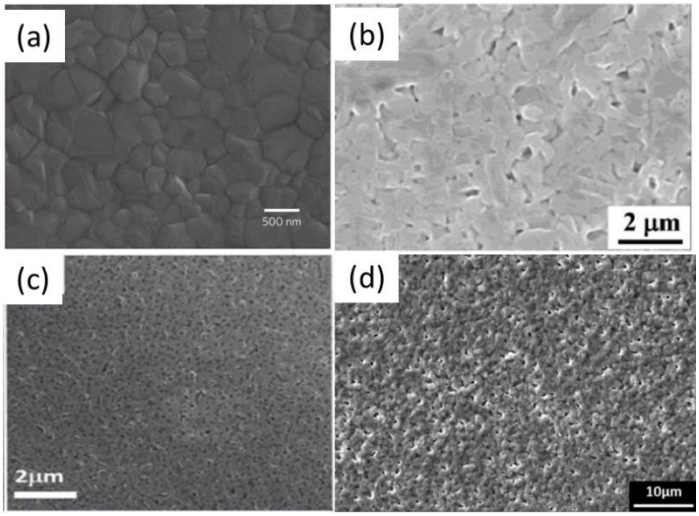

FIGURE 16. Top-view SEM images of perovskite layers: (a) $MAPbI_3$ deposited by two-step deposition method *via* MAI–PbI_2–DMSO intermediate phase; (b) $MAPbI_{3-x}Cl_x$ with 1% PEI; (c) $MAPbI_3$ with 2.8% of PFN; (d) $MAPbI_{3-x}Cl_x$ with 1% PEG. (a) Reprinted by permission from Macmillan Publishers Ltd: [54], copyright 2014. (b) Adapted from [100] with permission from The Royal Society of Chemistry, (c) Adapted from [97] with permission from The Royal Society of Chemistry, (d) Adapted with permission from [99]. Copyright 2015 American Chemical Society.

A notable example from Yao *et al* demonstrated incorporation of PEI as a cationic component directly into the perovskite crystal (Fig.17B).[101] Combined with the conventionally used MAI, uniform layers were formed with a smooth surface and an average grain size of 500 nm. No pinholes were observed on the surface, which explained high moisture resistivity of the resulting devices. The PCE was just marginally higher than that of control devices with a $MAPbI_3$ layer (15.2% against 14.6%), however stability remarkably increased. After 120 h of storage, the control device lost its performance completely, whereas the $(MAPbI_3)_{1-x}[(PEI)_2PbI_4]_x$ (x = 2%) device retained 92% of its initial PCE after 14 days of storage under ambient conditions.

As a templating agent, PMMA was shown to be not favourable since it did not form necessary non-covalent interactions with the hydrogen of the MA^+ cation.[97] However, it was successfully employed in growing homogenous crack-free mesoporous TiO_2 layers by the sol-gel method.[102,103] Deposition of TiO_2 from 40:60 PMMA:TiO isopropoxide solution resulted in the formation of a 170 nm thick porous film consisting of 20-30 nm nanoparticles covered by a thin layer of smaller particles (Fig.17A).[103] The films

formed from PS:TiO isopropoxide in similar conditions were not porous, so the mechanism of the pore formation is attributed solely to PMMA thermal depolymerisation, as suggested by Bywater.[104]

One of the major advantages of templating polymers is their low loadings, needed to achieve the maximum effect (1-2% is generally sufficient). Furthermore, the templating helps to decrease the deposition and annealing temperatures, while delivering perovskite films of high crystallinity, which in combination with low costs of the templating polymers explains their attractiveness for PSC industry.

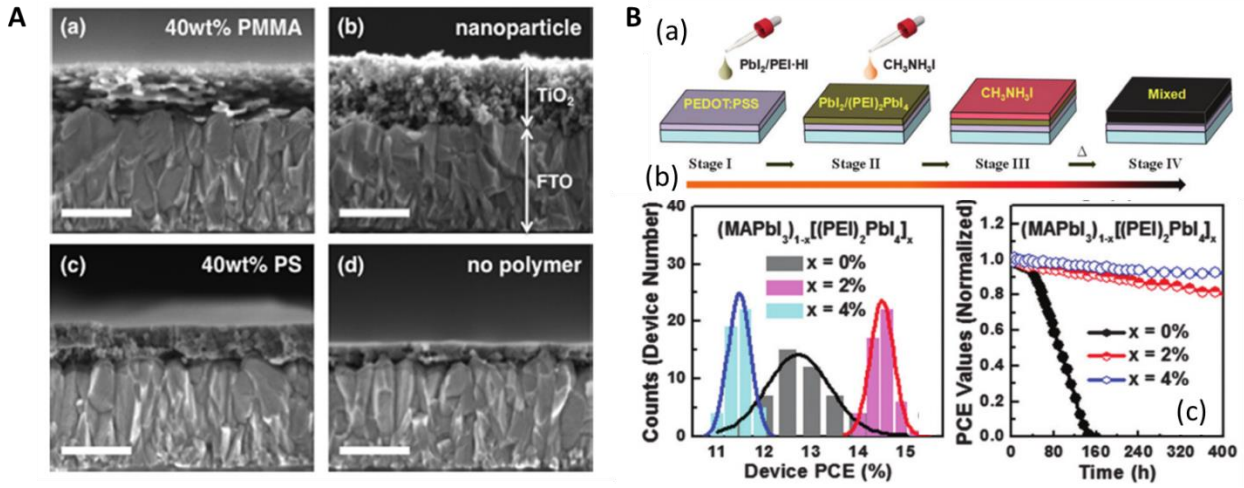

FIGURE 17. A. Cross-sectional SEM images of (a) TiO_2 (40 wt %-PMMA), (b) TiO_2 (nanoparticle), (c) TiO_2 (40 wt %-PS), and (d) TiO_2 (no polymer) on FTO/cTiO_2 substrates. Scale bars are 200 nm. Reprinted with permission from [103]. Copyright 2015 American Chemical Society. **B.** (a) Scheme of the two-step spin-coating procedure for mixed perovskite $(MAPbI_3)_{1-x}[(PEI)_2PbI_4]_x$. (b) Histogram of PCEs for each 50 devices and (c) stability of devices fabricated from layered perovskite of different compositions. Adapted from [101] with permission from The Royal Society of Chemistry.

5. Conclusions

Photovoltaic devices based on perovskite absorber have reached remarkable efficiencies within only three years of the first reports, and the reported values continue to increase, rendering the perovskite devices potential candidates to compete with conventional photovoltaic technologies. Combining the same advantageous properties/cost parameters with a far superior performance, PSCs already present a solid alternative to the OPV devices. Polymers, actually derived from previous OPV and OLED research have played one of the major roles in the perovskite success, providing various solutions for improvement:

from charge transport to quality of the absorber itself. There is a certain hope that the current obstacles preventing global implementation of the PSC technology can be addressed within reasonable timeframes by implementing advances and developments from other disciplines and relying on the experiences of OPV, OLED and DSSC communities. Polymers, in this case, encompass a large range of inexpensive strategic solutions that can be tuned according to their application, as demonstrated by the works discussed in this review.

Despite the achievements in performance, there are still unresolved issues preventing mass production of large area PSC modules. Firstly, more needs to be known about the stability of devices. During their evolution for more than two decades, OPV devices were thoroughly studied for their environmental and operational stability, and a lot of effort was put into improving their lifetime. PSCs, on the other hand, have been developing for only three years, and this short period has not been sufficient to collect enough evidence to confirm the degradation mechanisms or demonstrate that proposed solutions actually work. For example, most of the polymeric strategies that demonstrated improved stability of devices were not tested under operational conditions, but only in storage. As observed previously from OPV studies, operational conditions, such as light and elevated temperatures, give rise to other degradation mechanisms rather than those only occurring in storage.[64] Understandably, the primary concern has been the susceptibility of perovskite layer to moisture, which was a prominent feature of early perovskite devices.[105] However, since then, developments helped to overcome (to a certain extent) the moisture degradation effects by improving the perovskite layer quality and avoiding the pinholes and gaps between the perovskite grains.[19] Importantly, polymers substantially contributed to solving the moisture problem by providing barrier properties or serving as templating agents, as discussed in this review. Now it is necessary to explore, in more details, the effect of other stress factors (UV, temperatures, mechanical stress) on the overall device stability.

Furthermore, in most of the performed stability experiments, the storage conditions varied from study to study, demonstrating the need for a unified approach to stability studies. This problem existed in the OPV community until ISOS standards were introduced.[106] The same approach to establishing appropriate testing protocols (i.e., accelerated, operational, storage) is deemed necessary for PSCs.

The lack of testing protocols highlights another issue – the absence of a reliable standard control system. In OPVs, P3HT:PCBM bulk heterojunction served as a control system for years due to its rather robust behaviour and predictable PCE values. However, the diversity of systems in PSCs, and thus a huge variation in appropriate control systems, leaves an element of speculation in directly comparing independent reports. As a hot topic in current research, PSCs will undoubtedly give rise to such speculations,[107] as previously seen in OPV community.[108–110] The cooperation and agreement of different groups and laboratories helped to solve these issues in OPV research, and this is now an important direction where the research in PSCs should be taken to establish maximum scientific output without compromises in quality or completeness of obtained results.

Glossary

DPP(P)	poly[[2,5-bis(2-octyldo- decyl)-2,3,5,6-tetrahydro-3,6-dioxopyrrolo[3,4-c]pyrrole-1,4-diyl]-alt−[[2,2′-(2,5-thiophene)bis-thieno[3,2-b]thiophen]- 5,5′-diyl]]
ITO	indium tin oxide
Li-TFSI	bis(trifluoromethane)sulfonimide lithium
MEH-PPV	poly[2-methoxy-5-(2-ethylhexyloxy)-1,4-phenylenevinylene]
mp-TiO_2	mesoporous titanium oxide
P3HT	poly(3-hexylthiophene)
PANI	Polyaniline
PBDTTT-C	poly[(4,8-bis-(2-ethylhexyloxy)-benzo(1,2-b:4,5-b′)dithiophene)-2,6-diyl-alt-(4-(2-ethylhexanoyl)-thieno[3,4-b]thiophene)-2-6-diyl)]
PCBM	[6,6]-phenyl-C61-butyric acid methyl ester
PCBTDPP	poly[N-9-hepta-decanyl-2,7-carbazole-alt-3,6-bis-(thiophen-5-yl)-2,5-dioctyl-2,5-di-hydropyrrolo[3,4-]pyrrole-1,4-dione]
PCDTBT	poly[[9-(1-octylnonyl)-9H-carbazole-2,7-diyl]-2,5-thiophenediyl- 2,1,3-benzothiadiazole-4,7-diyl-2,5-thiophenediyl]
PCPDTBT	poly[2,1,3-benzothiadiazole-4,7-diyl[4,4-bis(2-ethylhexyl)-4H-cyclopenta[2,1-b:3,4-b′]dithiophene-2,6-diyl]]
PDPP3T	poly[{2,5-bis(2-hexyldecyl)-2,3,5,6-tetrahydro-3,6-dioxopyrrolo[3,4-c]pyrrole-1,4-diyl}-alt -{[2,2’:5’,2’’-terthiophene]-5,5’’-diyl}]
PDPPDBTE	poly[2,5-bis(2-octyldodecyl)pyrrolo[3,4-c]pyrrole-1,4(2H,5H)-dione-(E)-1,2-di(2,2'-bithiophen-5-yl)ethene]
PEDOT:PSS	poly(3,4-ethylenedioxythiophene):poly(4-styrene sulfonic acid)
PEO	poly(ethylene oxide)
PET	poly(ethylene terephthalate)

PFI	poly(tetrafluoroethylene-perfluoro-3,6-dioxa-4-methyl-7-octene-sulfonic acid)
PFN	poly[(9,9-bis(3'-(N,N-dimethylamino)propyl)-2,7-fluorene)-alt-2,7-(9,9–dioctylfluorene)]
PFN-OX	poly[9,9-bis(60-(N,N-diethylamino)propyl)-fluorene-alt-9,9-bis-(3- ethyl(oxetane-3-ethyloxy)-hexyl)-fluorene]
PFO	poly(9,9-di-n-octylfluorenyl-2,7-diyl)
PMMA	poly(methyl methacrylate)
PPDIDTT	poly{[N,N'-bis(2-decyl-tetradecyl)-3,4,9,10-perylenediimide-1,7-diyl]-alt-(dithieno[3,2-b:2',3'-d]thiophene-2,6-diyl)}
PS	polystyrene
PSS-*g*-PANI	poly(4-styrene sulfonate)-*graft*-polyaniline
PTB7	poly[[4,8-bis[(2-ethylhexyl)oxy]benzo[1,2-b:4,5-b']dithiophene-2,6-diyl][3-fluoro-2-[(2-ethylhexyl)carbonyl]thieno[3,4-b]thiophenediyl]]
PTB-DCB21	2'-butyloctyl-4,6-dibromo-3-fluorothieno[3,4-b]thiophene-2-carboxylate (TT-BO), 3',4'-dichlorobenzyl-4,6-dibromo-3-fluorothieno- [3,4-b]thiophene-2-carboxylate (TT-DCB), and 2,6-bis(trimethyl-tin)-4,8-bis(2-ethylhexyloxy)benzo[1,2-b:4,5-b']dithiophene (BDT-EH) copolymer
spiro-OMeTAD	N2,N2,N2′,N2′,N7,N7,N7′,N7′-octakis(4-methoxyphenyl)-9,9′-spirobi[9H-fluorene]-2,2′,7,7′-tetramine
TFB	poly[(9,9-dioctylfluorenyl-2,7-diyl)-co-(4,4′-(N-(4-sec-butylphenyl)diphenylamine)]
VNPB	N4,N4′-di(naphthalen-1-yl)-N4,N4′-bis(4-vinylphenyl)biphenyl-4,4′-diamine

Acknowledgements

AI acknowledges European Union Seventh Framework Programme (FP7/ 2011 under grant agreement ESTABLIS no. 290022) for financial support.

References

(1) Http://www.nrel.gov/ncpv/. NREL: National Center for Photovoltaics Home Page http://www.nrel.gov/ncpv/ (accessed Mar 7, 2016).

(2) Lee, M. M.; Teuscher, J.; Miyasaka, T.; Murakami, T. N.; Snaith, H. J. *Science* **2012**, *338* (6107), 643–647.

(3) Saparov, B.; Mitzi, D. B. *Chem. Rev.* **2016**, *116* (7), 4558–4596.

(4) Boix, P. P.; Nonomura, K.; Mathews, N.; Mhaisalkar, S. G. *Mater. Today* **2014**, *17* (1), 16–23.

(5) Niu, G.; Guo, X.; Wang, L. *J. Mater. Chem. A* **2015**, *3* (17), 8970–8980.

(6) Sum, T. C.; Mathews, N. *Energy Environ. Sci.* **2014**, *7* (8), 2518–2534.

(7) Park, N.-G. *Nano Converg.* **2016**, *3* (1), 15.

(8) Park, N.-G. *Mater. Today* **2015**, *18* (2), 65–72.

(9) Song, Z.; Watthage, S. C.; Phillips, A. B.; Heben, M. J. *J. Photonics Energy* **2016**, *6* (2), 22001.

(10) Kojima, A.; Teshima, K.; Shirai, Y.; Miyasaka, T. *J. Am. Chem. Soc.* **2009**, *131* (17), 6050–6051.

(11) Yuan, Y.; Huang, J.; Li, G. *Green* **2011**, *1* (1), 65–80.

(12) Meng, L.; You, J.; Guo, T. F.; Yang, Y. *Acc. Chem. Res.* **2016**, *49* (1), 155–165.

(13) Wu, C.-G.; Chiang, C.-H.; Tseng, Z.-L.; Nazeeruddin, M. K.; Hagfeldt, A.; Grätzel, M. *Energy Environ. Sci.* **2015**, *8* (9), 2725–2733.

(14) Heo, J. H.; Han, H. J.; Kim, D.; Ahn, T. K.; Im, S. H. *Energy Environ. Sci.* **2015**, *8* (5), 1602–1608.

(15) Bao, X.; Zhu, Q.; Qiu, M.; Yang, A.; Wang, Y.; Zhu, D.; Wang, J.; Yang, R. *J. Mater. Chem. A* **2015**, *3* (38), 19294–19298.

(16) Shao, Y.; Xiao, Z.; Bi, C.; Yuan, Y.; Huang, J. *Nat. Commun.* **2014**, *5*, 5784.

(17) Kim, H.-S.; Park, N.-G. *J. Phys. Chem. Lett.* **2014**, *5* (17), 2927–2934.

(18) Liu, C.; Fan, J.; Zhang, X.; Shen, Y.; Yang, L.; Mai, Y. *ACS Appl. Mater. Interfaces* **2015**, *7* (17), 9066–9071.

(19) Wang, D.; Wright, M.; Elumalai, N. K.; Uddin, A. *Sol. Energy Mater. Sol. Cells* **2016**, *147*, 255–275.

(20) Colladet, K.; Fourier, S.; Cleij, T. J.; Lutsen, L.; Gelan, J.; Vanderzande, D.; Nguyen, L. H.; Neugebauer, H.; Sariciftci, S.; Aguirre, A.; Janssen, G.; Goovaerts, E. *Macromolecules* **2007**, *40* (1), 65–72.

(21) Bundgaard, E.; Krebs, F. C. *Sol. Energy Mater. Sol. Cells* **2007**, *91* (11), 954–985.

(22) Topham, P. D.; Parnell, A. J.; Hiorns, R. C. *J. Polym. Sci. Part B-Polymer Phys.* **2011**, *49* (16), 1131–1156.

(23) Wantz, G.; Derue, L.; Dautel, O.; Rivaton, A.; Hudhomme, P.; Dagron-Lartigau, C. *Polym. Int.* **2014**, *63* (8), 1346–1361.

(24) Erothu, H.; Kolomanska, J.; Johnston, P.; Schumann, S.; Deribew, D.; Toolan, D. T. W.; Gregori, A.; Dagron-Lartigau, C.; Portale, G.; Bras, W.; Arnold, T.; Distler, A.; Hiorns, R. C.; Mokarian-Tabari, P.; Collins, T. W.; Howse, J. R.; Topham, P. D. *Macromolecules* **2015**, *48* (7), 2107–2117.

(25) Kim, H.-S.; Lee, C.; Im, J.-H.; Lee, K.-B.; Moehl, T.; Marchioro, A.; Moon, S.-J.; Humphry-baker, R.; Yum, J.-H.; Moser, J. E.; Gra, M. *Sci. Rep.* **2012**, *591*, 1–7.

(26) Shi, D.; Qin, X.; Li, Y.; He, Y.; Zhong, C.; Pan, J.; Dong, H.; Xu, W.; Li, T.; Hu, W.; Brédas, J.-L.; Bakr, O. M. *Sci. Adv.* **2016**, *2* (4), e1501491.

(27) Nguyen, W. H.; Bailie, C. D.; Unger, E. L.; McGehee, M. D. *J. Am. Chem. Soc.* **2014**, *136* (31), 10996–11001.

(28) Cappel, U. B.; Daeneke, T.; Bach, U. *Nano Lett.* **2012**, *12* (9), 4925–4931.

(29) Wang, S.; Yuan, W.; Meng, Y. S. *ACS Appl. Mater. Interfaces* **2015**, *7* (44), 24791–24798.

(30) Burschka, J.; Dualeh, A.; Kessler, F.; Baranoff, E.; Cevey-Ha, N.-L.; Yi, C.; Nazeeruddin, M. K.; Grätzel, M. *J. Am. Chem. Soc.* **2011**, *133* (45), 18042–18045.

(31) Burschka, J.; Kessler, F.; Nazeeruddin, M. K.; Grätzel, M. *Chem. Mater.* **2013**, *25* (15), 2986–2990.

(32) Xue, Q.; Chen, G.; Liu, M.; Xiao, J.; Chen, Z.; Hu, Z.; Jiang, X. F.; Zhang, B.; Huang, F.; Yang, W.; Yip, H. L.; Cao, Y. *Adv. Energy Mater.* **2015**, 1–9.

(33) Huang, X.; Wang, K.; Yi, C.; Meng, T.; Gong, X. *Adv. Energy Mater.* **2015**, No. 6, 1501773.

(34) Long, M.; Chen, Z.; Zhang, T.; Xiao, Y.; Zeng, X.; Chen, J.; Yan, K.; Xu, J. *Nanoscale* **2016**, 6290–6299.

(35) Guo, Y.; Liu, C.; Inoue, K.; Harano, K.; Tanaka, H.; Nakamura, E. *J. Mater. Chem. A* **2014**, *2* (34), 13827–13830.

(36) Wang, J. Y.; Hsu, F. C.; Huang, J. Y.; Wang, L.; Chen, Y. F. *ACS Appl. Mater. Interfaces* **2015**, *7* (50), 27676–27684.

(37) Conings, B.; Baeten, L.; De Dobbelaere, C.; D'Haen, J.; Manca, J.; Boyen, H. G. *Adv. Mater.* **2014**, *26* (13), 2041–2046.

(38) Chang, S. H.; Lin, K.-F.; Chiu, K. Y.; Tsai, C.-L.; Cheng, H.-M.; Yeh, S.-C.; Wu, W.-T.; Chen, W.-N.; Chen, C.-T.; Chen, S.-H.; Wu, C.-G. *Sol. Energy* **2015**, *122* (11), 892–899.

(39) Xiong, J.; Yang, B.; Wu, R.; Cao, C.; Huang, Y.; Liu, C.; Hu, Z.; Huang, H.; Gao, Y.; Yang, J. *Org. Electron.* **2015**, *24*, 106–112.

(40) Sin, D. H.; Ko, H.; Jo, S. B.; Kim, M.; Bae, G. Y.; Cho, K. *ACS Appl. Mater. Interfaces* **2016**, *8* (10), 6546–6553.

(41) Liu, C.; Su, Z.; Li, W.; Jin, F.; Chu, B.; Wang, J.; Zhao, H.; Lee, C. S.; Tang, J.; Kang, B. *Org. Electron.* **2016**, *33*, 221–226.

(42) Li, D.; Cui, J.; Li, H.; Huang, D.; Wang, M.; Shen, Y. *Sol. Energy* **2016**, *131*, 176–182.

(43) Lim, K.-G.; Kim, H.-B.; Jeong, J.; Kim, H.; Kim, J. Y.; Lee, T.-W. *Adv. Mater.* **2014**, *26* (37), 6461–6466.

(44) Xiao, Y.; Han, G.; Wu, J.; Lin, J. Y. *J. Power Sources* **2016**, *306*, 171–177.

(45) Zhu, Q.; Bao, X.; Yu, J.; Zhu, D.; Qiu, M.; Yang, R.; Dong, L. *ACS Appl. Mater. Interfaces* **2016**, *8* (4), 2652–2657.

(46) Du, Y.; Cai, H.; Ni, J.; Li, J.; Yu, H.; Sun, X.; Wu, Y.; Wen, H.; Zhang, J. *RSC Adv.* **2015**, *5* (82), 66981–66987.

(47) Heo, J. H.; Im, S. H.; Noh, J. H.; Mandal, T. N.; Lim, C.-S.; Chang, J. A.; Lee, Y. H.; Kim, H.; Sarkar, A.; NazeeruddinMd, K.; Gratzel, M.; Seok, S. Il. *Nat Phot.* **2013**, *7* (6), 486–491.

(48) Dubey, A.; Adhikari, N.; Venkatesan, S.; Gu, S.; Khatiwada, D.; Wang, Q.; Mohammad, L.; Kumar, M.; Qiao, Q. *Sol. Energy Mater. Sol. Cells* **2016**, *145*, 193–199.

(49) Kwon, Y. S.; Lim, J.; Yun, H.-J.; Kim, Y.-H.; Park, T. *Energy Environ. Sci.* **2014**, *7* (4), 1454.

(50) Chen, W.; Bao, X.; Zhu, Q.; Zhu, D.; Qiu, M.; Sun, M.; Yang, R. *J. Mater. Chem. C* **2015**, *3* (39), 10070–10073.

(51) Lee, J.-W.; Park, S.; Ko, M. J.; Son, H. J.; Park, N.-G. *Chemphyschem* **2014**, *15* (12), 2595–2603.

(52) Wang, Z.; Dong, Q.; Xia, Y.; Yu, H.; Zhang, K.; Liu, X.; Guo, X.; Zhou, Y.; Zhang, M.; Song, B. *Org. Electron.* **2016**, *33*, 142–149.

(53) Zhu, Z.; Bai, Y.; Lee, H. K. H.; Mu, C.; Zhang, T.; Zhang, L.; Wang, J.; Yan, H.; So, S. K.; Yang, S. *Adv. Funct. Mater.* **2014**, *24* (46), 7357–7365.

(54) Jeon, N. J.; Noh, J. H.; Kim, Y. C.; Yang, W. S.; Ryu, S.; Seok, S. Il. *Nat. Mater.* **2014**, *13* (9),

897–903.

(55) Jeon, N. J.; Noh, J. H.; Yang, W. S.; Kim, Y. C.; Ryu, S.; Seo, J.; Seok, S. Il. *Nature* **2015**, *517* (7535), 476–480.

(56) Yang, W. S.; Noh, J. H.; Jeon, N. J.; Kim, Y. C.; Ryu, S.; Seo, J.; Seok, S. Il. *Science (80-.).* **2015**, *348* (6240), 1234–1237.

(57) Malinkiewicz, O.; Yella, A.; Lee, Y. H.; Espallargas, G. M. M.; Graetzel, M.; Nazeeruddin, M. K.; Bolink, H. J. *Nat. Photonics* **2014**, *8* (2), 128–132.

(58) Neumann, K.; Thelakkat, M. *RSC Adv.* **2014**, *4* (82), 43550–43559.

(59) Xu, J.; Voznyy, O.; Comin, R.; Gong, X.; Walters, G.; Liu, M.; Kanjanaboos, P.; Lan, X.; Sargent, E. H. *Adv. Mater.* **2016**, *28*, 2807–2815.

(60) Ameen, S.; Akhtar, M. S.; Seo, H.-K.; Shin, H.-S. *Langmuir* **2014**, *30* (43), 12786–12794.

(61) Lim, K.-G.; Ahn, S.; Kim, H.; Choi, M.-R.; Huh, D. H.; Lee, T.-W. *Adv. Mater. Interfaces* **2016**, *3* (9), 1500678.

(62) Timpanaro, S.; Kemerink, M.; Touwslager, F. J.; De Kok, M. M.; Schrader, S. *Chem. Phys. Lett.* **2004**, *394* (4), 339–343.

(63) You, J.; Yang, Y. (Michael); Hong, Z.; Song, T.-B.; Meng, L.; Liu, Y.; Jiang, C.; Zhou, H.; Chang, W.-H.; Li, G.; Yang, Y. *Appl. Phys. Lett.* **2014**, *105* (18), 183902.

(64) Grossiord, N.; Kroon, J.; Andriessen, R.; Blom, P. *Org. Electron.* **2012**, *13* (3), 432–456.

(65) Zhang, S.; Yu, Z.; Li, P.; Li, B.; Isikgor, F. H.; Du, D.; Sun, K.; Xia, Y.; Ouyang, J. *Org. Electron.* **2016**, *32*, 149–156.

(66) Li, J.-F.; Zhao, C.; Zhang, H.; Tong, J.-F.; Zhang, P.; Yang, C.-Y.; Xia, Y.-J.; Fan, D.-W. *Chinese Phys. B* **2016**, *25* (2), 28402.

(67) Hou, F.; Su, Z.; Jin, F.; Yan, X.; Wang, L.; Zhao, H.; Zhu, J.; Chu, B.; Li, W. *Nanoscale* **2015**, *7* (21), 9427–9432.

(68) Kline, R. J.; McGehee, M. D.; Kadnikova, E. N.; Liu, J.; Fréchet, J. M. J. *Adv. Mater.* **2003**, *15* (18), 1519–1522.

(69) Kline, R. J.; McGehee, M. D.; Kadnikova, E. N.; Liu, J.; Fre, J. M. J.; Toney, M. F. *Macromolecules* **2005**, *38* (8), 3312–3319.

(70) Yang, X.; Chueh, C.-C.; Li, C.-Z.; Yip, H.-L.; Yin, P.; Chen, H.; Chen, W.-C.; Jen, A. K.-Y. *Adv. Energy Mater.* **2013**, *3* (5), 666–673.

(71) Lu, L.; Luo, Z.; Xu, T.; Yu, L. *Nano Lett.* **2013**, *13* (1), 59–64.

(72) In, S.; Mason, D. R.; Lee, H.; Jung, M.; Lee, C.; Park, N. *ACS Photonics* **2015**, *2* (1), 78–85.

(73) Jhuo, H.-J.; Yeh, P.-N.; Liao, S.-H.; Li, Y.-L.; Cheng, Y.-S.; Chen, S.-A. *J. Chinese Chem. Soc.* **2014**, *61* (1), 115–126.

(74) Cai, B.; Xing, Y. D.; Yang, Z.; Zhang, W. H.; Qiu, J. S. *Energy Environ. Sci.* **2013**, *6* (5), 1480–1485.

(75) *Polyfluorenes*; Scherf, U., Neher, D., Eds.; Advances in Polymer Science; Springer Berlin Heidelberg: Berlin, Heidelberg, 2008; Vol. 212.

(76) Thelakkat, M.; Hagen, J.; Haarer, D.; Schmidt, H.-W. *Synth. Met.* **1999**, *102* (1–3), 1125–1128.

(77) Hüttner, S.; Sommer, M.; Steiner, U.; Thelakkat, M. *Appl. Phys. Lett.* **2010**, *96* (7), 73503.

(78) Huang, F.; Chen, K.-S.; Yip, H.-L.; Hau, S. K.; Acton, O.; Zhang, Y.; Luo, J.; Jen, A. K.-Y. *J. Am. Chem. Soc.* **2009**, *131* (39), 13886.

(79) Madec, M.-B.; Morrison, J. J.; Rabjohns, M.; Turner, M. L.; Yeates, S. G. *Org. Electron.* **2010**, *11* (4), 686–691.

(80) Ma, W.; Kim, J. Y.; Lee, K.; Heeger, A. J. *Macromol. Rapid Commun.* **2007**, *28* (17), 1776–1780.

(81) Ego, C.; Grimsdale, A. C.; Uckert, F.; Yu, G.; Srdanov, G.; Müllen, K. *Adv. Mater.* **2002**, *14* (11), 809–811.

(82) Koh, T. M.; Fu, K.; Fang, Y.; Chen, S.; Sum, T. C.; Mathews, N.; Mhaisalkar, S. G.; Boix, P. P.; Baikie, T. *J. Phys. Chem. C* **2014**, *118* (30), 16458–16462.

(83) Rannou, P.; Nechtschein, M. *Synth. Met.* **1997**, *84* (1–3), 755–756.

(84) Focke, W.; Wnek, G.; Wei, Y. *J. Phys. Chem.* **1987**, *91* (7), 5813–5818.

(85) Choi, M.-R.; Woo, S.-H.; Han, T.-H.; Lim, K.-G.; Min, S.-Y.; Yun, W. M.; Kwon, O. K.; Park, C. E.; Kim, K.-D.; Shin, H.-K.; Kim, M.-S.; Noh, T.; Park, J. H.; Shin, K.-H.; Jang, J.; Lee, T.-W. *ChemSusChem* **2011**, *4* (3), 363–368.

(86) Liu, Y.; Renna, L. A.; Page, Z. A.; Thompson, H. B.; Kim, P. Y.; Barnes, M. D.; Emrick, T.; Venkataraman, D.; Russell, T. P. *Adv. Energy Mater.* **2016**, *6* (20), 1600664.

(87) Abrusci, A.; Stranks, S. D.; Docampo, P.; Yip, H.-L.; Jen, A. K.-Y.; Snaith, H. J. *Nano Lett.* **2013**, *13* (7), 3124–3128.

(88) Xue, Q.; Hu, Z.; Liu, J.; Lin, J.; Sun, C.; Chen, Z.; Duan, C.; Wang, J.; Liao, C.; Lau, W. M.; Huang, F.; Yip, H.-L.; Cao, Y. *J. Mater. Chem. A* **2014**, *2* (46), 19598–19603.

(89) Hu, Q.; Liu, Y.; Li, Y.; Lei, Y.; Liu, T.; Huang, F.; Wang, S.; Huang, W.; Zhu, R.; Gong, Q. *J. Mater. Chem. A* **2015**, 18483–18491.

(90) Sun, C.; Wu, Z.; Yip, H. L.; Zhang, H.; Jiang, X. F.; Xue, Q.; Hu, Z.; Hu, Z.; Shen, Y.; Wang, M.; Huang, F.; Cao, Y. *Adv. Energy Mater.* **2015**, 1–10.

(91) Wang, W.; Yuan, J.; Shi, G.; Zhu, X.; Shi, S.; Liu, Z.; Han, L.; Wang, H.-Q.; Ma, W. *ACS Appl. Mater. Interfaces* **2015**, *7* (7), 3994–3999.

(92) Seo, Y. H.; Yeo, J. S.; Myoung, N.; Yim, S. Y.; Kang, M.; Kim, D. Y.; Na, S. I. *ACS Appl. Mater. Interfaces* **2016**, *8* (20), 12822–12829.

(93) Meng, F.; Liu, K.; Dai, S.; Shi, J.; Zhang, H.; Xu, X.; Li, D.; Zhan, X. *Mater. Chem. Front.* **2017**.

(94) Chiang, C.-H.; Wu, C.-G. *Nat. Photonics* **2016**, *10* (3), 196–200.

(95) Chen, Y.; He, M.; Peng, J.; Sun, Y.; Liang, Z. *Adv. Sci.* **2016**, *3* (4), 1500392.

(96) Ding, Y.; Yao, X.; Zhang, X.; Wei, C.; Zhao, Y. *J. Power Sources* **2014**, *272*, 351–355.

(97) Masi, S.; Rizzo, A.; Aiello, F.; Balzano, F.; Uccello-Barretta, G.; Listorti, A.; Gigli, G.; Colella, S. *Nanoscale* **2015**, *7* (45), 18956–18963.

(98) Masi, S.; Colella, S.; Listorti, A.; Roiati, V.; Liscio, A.; Palermo, V.; Rizzo, A.; Gigli, G. *Sci. Rep.* **2015**, *5*, 7725.

(99) Chang, C.-Y.; Chu, C.-Y.; Huang, Y.-C.; Huang, C.-W.; Chang, S.-Y.; Chen, C.-A.; Chao, C.-Y.; Su, W.-F. *ACS Appl. Mater. Interfaces* **2015**, *7* (8), 4955–4961.

(100) Dong, Q.; Wang, Z.; Zhang, K.; Yu, H.; Huang, P.; Liu, X.; Zhou, Y.; Chen, N.; Song, B.

Nanoscale **2016**, 5552–5558.

(101) Yao, K.; Wang, X.; Li, F.; Zhou, L. *Chem. Commun.* **2015**, *51*, 15430–15433.

(102) Jin, M.; Kim, S. S.; Yoon, M.; Li, Z.; Lee, Y. Y.; Kim, J. M. *J. Nanosci. Nanotechnol.* **2012**, *12* (1), 815–821.

(103) Yue, Y.; Umeyama, T.; Kohara, Y.; Kashio, H.; Itoh, M.; Ito, S.; Sivaniah, E.; Imahori, H. *J. Phys. Chem. C* **2015**, *119* (40), 22847–22854.

(104) Bywater, S.; Black, P. E. *J. Phys. Chem.* **1965**, *69* (9), 2967–2970.

(105) Grätzel, M. *Nat. Mater.* **2014**, *13* (9), 838–842.

(106) Reese, M. O.; Gevorgyan, S. A.; Jørgensen, M.; Bundgaard, E.; Kurtz, S. R.; Ginley, D. S.; Olson, D. C.; Lloyd, M. T.; Morvillo, P.; Katz, E. A.; Elschner, A.; Haillant, O.; Currier, T. R.; Shrotriya, V.; Hermenau, M.; Riede, M.; R. Kirov, K.; Trimmel, G.; Rath, T.; Inganäs, O.; Zhang, F.; Andersson, M.; Tvingstedt, K.; Lira-Cantu, M.; Laird, D.; McGuiness, C.; Gowrisanker, S. (Jimmy); Pannone, M.; Xiao, M.; Hauch, J.; Steim, R.; DeLongchamp, D. M.; Rösch, R.; Hoppe, H.; Espinosa, N.; Urbina, A.; Yaman-Uzunoglu, G.; Bonekamp, J.-B.; van Breemen, A. J. J. M.; Girotto, C.; Voroshazi, E. *Sol. Energy Mater. Sol. Cells* **2011**, *95* (5), 1253–1267.

(107) Editorial. *Nat Mater* **2014**, *13* (9), 837.

(108) Snaith, H. J. *Nat. Photonics* **2012**, *6*, 337–340.

(109) Editorial. *Nat. Photonics* **2014**, *8* (9), 665–665.

(110) Zimmermann, E.; Ehrenreich, P.; Pfadler, T.; Dorman, J. A.; Weickert, J.; Schmidt-Mende, L. *Nat. Photonics* **2014**, *8* (9), 669–672.